National Defence / Défense nationale

EFFECTS OF IMBALANCES AND DC OFFSETS ON I/Q DEMODULATION (U)

by

Jim P.Y. Lee

DEFENCE RESEARCH ESTABLISHMENT OTTAWA

REPORT NO. 1148

Canada

December 1992
Ottawa

National Defence / Défense nationale

EFFECTS OF IMBALANCES AND DC OFFSETS ON I/Q DEMODULATION (U)

by

Jim P.Y. Lee
Radar ESM Section
Electronic Warfare Division

DEFENCE RESEARCH ESTABLISHMENT OTTAWA
REPORT NO. 1148

PCN
011LB

December 1992
Ottawa

ABSTRACT

The effects of imbalances and DC offsets, in an I/Q demodulator, on the demodulation of radar signals are addressed in this report. Three normalized parameters, namely the peak–to–peak–ripple to mean ratio, phase error and normalized instantaneous frequency deviation are used to characterize distortions introduced on the envelope, phase and instantaneous frequency respectively. The effect on the distortions due to aliasing and an approximation used in deriving the instantaneous frequency in a discrete–time processor, is also analyzed.

When there are imbalances and DC offsets, a bias is produced on both the demodulated envelope and phase. AC ripples with frequency components which are multiples of the baseband frequency are also generated on all of the three demodulated waveforms. Since the demodulated waveform bandwidth is usually much narrower than the instantaneous bandwidth of the I/Q demodulator and at high baseband frequency, the high frequency components of the distortions can be effectively reduced by low–pass filtering.

RESUME

Ce rapport contient une analyse des effets des asymétries et des niveaux de courant continu sur un démodulateur en quadrature de phase. Les distorsions de l'enveloppe, de la phase et de la fréquence instantanée de signaux radar, sont analysées, respectivement, à l'aide de trois paramètres normalisés, soient le rapport, crête–à–crête, des fluctuations à la moyenne de l'enveloppe, l'erreur de phase et les changements de fréquence instantanée. On y analyse aussi l'impact sur les distorsions du repliement spectral et des approximations utilisées dans la détermination de la fréquence instantanée par un système de traitement à échantillonnage temporel.

Les asymétries et les décalages de courant continu produisent un biais qui s'ajoute à l'enveloppe démodulée et à la phase. Des fluctuations de courant alternatif contenant des composantes spectrales situées aux multiples de la fondamentale sont générées pour les trois signaux démodulés. Pour les applications de guerre électronique, la bande passante du démodulateur en quadrature est habituellement beaucoup plus grande que la bande passante du signal démodulé. Lorsque la fondamentale du signal est grande et comparable à sa largeur de bande de modulation, les composantes à haute fréquence de la distorsion peuvent être atténuées efficacement par un filtre passe–bas.

EXECUTIVE SUMMARY

Due to the increasing density and complexity of radar signal waveforms, it is becoming difficult to sort out and identify each radar emitter uniquely using conventional signal parameters such as pulse width, radio frequency (RF), amplitude and pulse repetition frequency. As a result, in electronic warfare applications, there is a requirement for a radar Electronic Support Measures (ESM) receiver to measure precisely the modulation characteristics of radar signals and to provide additional parameters on the modulation waveform such as envelope, phase and instantaneous frequency which can be used to identify unambiguously each type of radar emitter. With the advent of fast A/D converters and high–speed digital signal processing technologies, I/Q demodulators have been developed which can measure accurately the modulation characteristics of radar signals.

There are different approaches in the implementation of an I/Q demodulator. The most common one is the conventional I/Q demodulator where the generation of the in–phase and quadrature components of a signal is implemented using analog components. The in–phase and quadrature signals are then digitized and processed to extract the modulation characteristics of the signal. The attractive features of this approach are its wide instantaneous bandwidth and simple implementation. However, there are amplitude and phase imbalances between the two channels and DC offset in each channel, which in turn can introduce systematic errors to the measurement.

Other digital approaches of directly eliminating the mismatches have also been proposed. In these approaches, the splitting of the input signal into its in–phase and quadrature components is carried out in the digital domain by passing the digital signal through digital Hilbert transform filters. However, the computational load of the digital processor is increased due to the requirements of the digital filtering operations and some distortion is also introduced due to finite word length effects and the finite order of the digital filters. The magnitude and type of mismatches depend on the particular scheme implemented. In general, the imbalances and DC offsets can be made much less than the conventional I/Q demodulator implemented using commercial quadrature mixers.

No matter which approach is used, some form of mismatch does exist in the generation of the in–phase and quadrature signals. This will inevitably affect the accuracy of the demodulated information.

The purpose of this report is two–fold. The first objective is to analyze the effects of imbalance errors and DC offsets on the demodulated characteristics. Different cases in terms of the imbalances and DC offsets are used to illustrate the distortions introduced. The second objective is to present simple techniques which can be used to reduce the distortions introduced by the imbalances and DC offsets.

The effects of imbalances and DC offsets, in an I/Q demodulator, on the demodulation of radar signals are addressed. Three normalized parameters, namely the peak–to–peak–ripple to mean, phase error and normalized instantaneous frequency deviation are used to characterize distortions introduced on the envelope, phase and instantaneous frequency respectively. The effect on the distortions, due to aliasing and an approximation used in deriving the instantaneous frequency in a discrete–time processor, is also analyzed.

When there are imbalances and DC offsets, a bias is produced on both the demodulated envelope and phase. AC ripples with frequency components which are multiples of the baseband frequency are also generated on all of the three demodulated waveforms. In EW applications, the video or modulation bandwidth of the signal is usually small in comparison to the instantaneous frequency bandwidth of the I/Q demodulator. As a result, when the signal is down–converted to a baseband frequency which is larger than the modulation bandwidth, the frequency components of the distortions can be reduced by low–pass filtering. The technique of using a moving average has been shown to be effective to attenuate the ripples caused by the mismatches and with minimal effect on both the demodulated envelope and instantaneous frequency.

TABLE OF CONTENTS

1.0 INTRODUCTION

Due to the increasing density and complexity of radar signal waveforms, it is becoming very difficult to sort out and identify each radar emitter uniquely using conventional signal parameters such as pulse width, radio frequency (RF), amplitude and pulse repetition frequency. As a result, in electronic warfare applications, there is a requirement for a radar Electronic Support Measures (ESM) receiver to measure precisely the modulation characteristics of radar signals and to provide additional parameters on the modulation waveform such as amplitude, phase and frequency which can be used to identify unambiguously each type of radar emitter. With the advent of fast A/D converters and high–speed digital signal processing technologies, it is possible to develop digital microwave receivers which can meet this requirement [1].

A simple conventional in–phase/quadrature (I/Q) demodulator which can measure accurately the envelope, phase and instantaneous frequency of radar signals is shown in Fig. 1. The attractive features of this architecture for radar ESM applications are: (i) wide instantaneous bandwidth because the negative and positive frequencies with respect to the local oscillator frequency can be distinguished, and (ii) simple algorithms for the extraction of modulation characteristics can be used so that nearly real–time results can be obtained.

Wide instantaneous bandwidth is important for a number of reasons. In EW applications, the signal frequency bandwidth can be large and 500 MHz is not uncommon [2]. In addition, if it is required to measure fine modulations of narrow pulses, a wide instantaneous bandwidth with minimal group delay variations is also needed. Furthermore, the frequencies of the signals of interest are usually unknown and they may scatter in a much broader frequency band than the bandwidths of the signals. As a result, in this case the instantaneous bandwidth of an I/Q demodulator is usually designed to be much wider than the modulation bandwidths of the signals.

The conventional I/Q approach has its own problem. Because the splitting of the signal into its in–phase and quadrature components is implemented using analog components, there are amplitude and phase imbalances between the two channels and DC offset in each channel, which in turn can introduce systematic errors to the measurement[3–6]. Quadrature mixers are commercially available, however they exhibit relatively large amplitude and phase imbalances[6,7]. On the other hand, much better matching characteristics can be obtained by using custom–matched quadrature mixers[6]. The imbalances and DC offsets of I/Q demodulators can also be reduced in the processing by using calibration and compensation techniques[6,8]

Other approaches of directly eliminating the mismatches have been proposed recently [9–12]. In these approaches, the bandpass signal is either directly sampled or is first down converted to a lower intermediate frequency (IF) before it is sampled. The splitting of the input signal into its in–phase and quadrature components is carried out in the digital domain by passing the digital signal through digital Hilbert transform filters. However, the computational load of the digital processor is increased due to the additional requirements of the digital filtering operations and some distortion is also introduced due to finite word length effects and the finite order of the digital filters. The magnitude and type of mismatches depend on the particular scheme implemented. In general, the

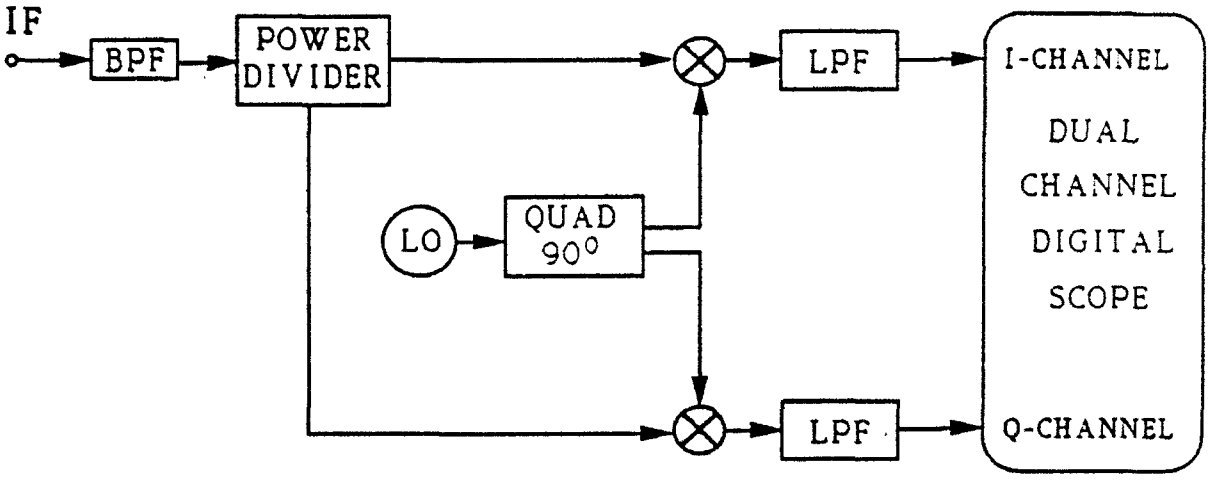

Figure 1 Block Diagram of Conventional I/Q Demodulator

imbalances and DC offsets can be made much less than the conventional I/Q demodulator implemented using commercial quadrature mixers.

No matter which approach is used, some form of mismatch does exist in the generation of the in–phase and quadrature signals. This will inevitably affect the accuracy of the demodulated information.

In EW applications, the envelope, phase and instantaneous frequency of the signal modulation are measured directly, and consequently, the effects of imbalances and DC offsets on the demodulated waveforms as a function of time are of interest. As a result, the analysis carried out in this report is focused on the time domain effects which are different from the conventional approach [3–5] where the effects are characterized in the frequency domain in terms of the relative ratio of the demodulated signal frequency to its image frequency. The analysis given in this report is based mainly on the use of the conventional I/Q demodulator. For other digital approaches, the generation of the in–phase and quadrature components may be different, but the effects of imbalances and DC offsets on the demodulated signals are equally applicable.

The purpose of this report is two–fold. The first objective is to analyze the effects of imbalance errors and DC offsets on the demodulation characteristics. Different cases in terms of the imbalances and DC offsets are used to illustrate the distortions introduced. The second objective is to present simple techniques which can be used to reduce the distortions introduced by the imbalances and DC offsets.

2.0 I/Q DEMODULATION

An incoming RF signal is usually down–converted to an IF signal before it is applied to the I/Q demodulator. The IF signal applied to the I/Q demodulator can be expressed in the form of

$$s(t) = a(t)\cos[\omega_o t + \phi(t)] \tag{1}$$

where $a(t)$ is the amplitude or envelope, ω_o is the IF angular carrier frequency and $\phi(t)$ is the phase function of the signal. In a conventional I/Q demodulator as shown in Fig. 1 , the signal is first bandpass filtered and then equally power–divided into two paths. The signal in each path is then mixed down to baseband by the use of a local oscillator signal. The two local oscillator signals are derived from the same source, but are 90 degrees out of phase. The resultant in–phase and quadrature baseband signals after the low–pass filter (LPF) are,

$$S_i(t) = K/2\ a(t)\cos[(\omega_o - \omega_{lo})t + \phi(t) - \gamma] = K/2\ a(t)\cos[\beta(t)] \tag{2}$$

and

$$S_q(t) = K/2\ a(t)\sin[\beta(t)] \tag{3}$$

respectively, where K is the net gain in each path , ω_{lo} is the angular frequency of the local oscillator with initial phase γ, $\beta(t)$ is the phase function of the baseband signal and a constant delay introduced in each path has been neglected. In this ideal case, the two

channels have been assumed to be perfectly matched in amplitude, 90 degrees out of phase and with no DC offsets.

The instantaneous power of the envelope of the input IF signal is simply related to its in–phase and quadrature baseband components by

$$a^2(t) = 4/K^2 \left[S_i^2(t) + S_q^2(t) \right], \tag{4}$$

the signal phase function is given by

$$\begin{aligned} \phi(t) &= \beta(t) - (\omega_o - \omega_{lo})t + \gamma \\ &= \tan^{-1} [S_q(t)/S_i(t)] - (\omega_o - \omega_{lo})t + \gamma \end{aligned} \tag{5}$$

and the instantaneous angular frequency is

$$2\pi f(t) = \frac{d\phi(t)}{dt} = \frac{d}{dt} \left[\tan^{-1} [S_q(t)/S_i(t)] \right] - (\omega_o - \omega_{lo}). \tag{6}$$

The in–phase and quadrature baseband signals are usually sampled and quantized at $t_n = nT_s + T_o$, where T_s is the sampling interval, T_o is the initial time and $n = 0,1,2,\ldots$. In this case, the sampled instantaneous angular frequency is then approximately given by

$$2\pi f(t_n) \approx \left[\phi(t_n) - \phi(t_{n-1}) \right] / T_s \tag{7}$$

3.0 AMPLITUDE AND PHASE IMBALANCES AND DC OFFSETS

In the implementation of the I/Q demodulator there will be differential gain, DC offsets and phase deviation from the ideal 90 degrees between the two channels [4]. Equations (2) and (3) can then be rewritten in a more general form as

$$S_i(t) = K_i/2 \; a(t) \cos[\beta(t) + \phi_i] + a_{io} \tag{8}$$

and

$$S_q(t) = K_q/2 \; a(t) \sin[\beta(t) + \phi_q] + a_{qo} \tag{9}$$

respectively, where a_{io} and a_{qo} are the amplitude DC offsets, K_i and K_q are the gains, and ϕ_i and ϕ_q are the phases of the in–phase and quadrature channels respectively. a_{io}, a_{qo}, K_i, K_q ,ϕ_i and ϕ_q are in general a function of frequency. For narrow–band signals, they can be assumed to be approximately constant.

There are four basic components on the mismatches, namely amplitude imbalance, phase imbalance and DC offsets in the in–phase channel and quadrature channel. Depending on the type of I/Q demodulator or the digital approach used, the relative magnitude of the four mismatch components can vary. In the conventional I/Q

demodulator, if commercial quadrature mixers are used, all four components can be large. If a custom–matched quadrature mixer is used, the imbalances can be quite small. If the DC offsets are stored and subtracted digitally from the in–phase and quadrature signals in the processing, then DC offsets are negligible as compared to the imbalances. In the digital approach, if one Hilbert transformer is used in one of the channels in generating the quadrature component[9], only amplitude imbalance and one DC offset are present. If two linear–phase FIR bandpass filters with frequency responses identical in amplitude but 90 degrees shifted in phase, the DC offsets will be eliminated and the amplitude and phase imbalances are then determined by the finite number of bits in the A/D converters and the sampling jitter [12].

The general case in which all the imbalances and DC offsets are present is discussed. In addition, other specific cases are also analyzed in detail. The specific cases presented in this report are :

(i) Amplitude and Phase Imbalances Only,
(ii) Amplitude Imbalance Only,
(iii) Phase Imbalance Only,
(iv) DC Offsets Only and
(v) Amplitude and DC Offset Only

3.1 Envelope Measurement

From Eqs.(8) and (9), the instantaneous power of the envelope of the baseband signal can be shown to be

$$S_i^2(t) + S_q^2(t) = [a(t)K_i]^2/4 \left\{ 1/2 + \{a_{io}/[a(t)K_i/2]\}^2 + R^2/2 + \{a_{qo}/[a(t)K_i/2]\}^2 \right.$$
$$+ \left[2\, a_{io}/[a(t)K_i/2] \cos[\alpha_o(t)] + 2\, R\, a_{qo}/[a(t)K_i/2] \sin[\alpha_o(t) + \Delta\phi] \right]$$
$$\left. + \left[1/2 \cos[2\alpha_o(t)] - R^2/2 \cos[2\alpha_o(t) + 2\Delta\phi\,] \right] \right\} \tag{10}$$

where $\alpha_o(t) = \beta(t) + \phi_i$ (11)

is the input phase function of the baseband signal with a constant phase offset ϕ_i.

The calculated envelope has been expressed in terms of relative and normalized parameters, with

$$R = K_q/K_i \tag{12}$$

as the amplitude imbalance ratio,

$$\Delta\phi = (\phi_q - \phi_i) \tag{13}$$

as the phase imbalance,

$$a_{io}/[a(t)K_i/2] \tag{14}$$

and

$$a_{qo}/[a(t)K_i/2] \tag{15}$$

as the normalized DC offsets of the in–phase and quadrature channels respectively. It has also been expressed as a product of the undistorted envelope term $\{[a(t)K_i]^2/4\}$ and a sum of other terms which are generated by the imbalances and DC offsets. When the two channels are perfectly matched, the sum of all the terms inside the braces is unity. By dividing both sides of Eq.(10) by $\{[a(t)K_i]^2/4\}$, the normalized envelope is simply given by the terms inside the braces. A DC term other than unity indicates a change in magnitude of the undistorted envelope while an AC term also indicates a change in shape. In the frequency domain, the spectrum of the undistorted envelope is affected only in magnitude by the DC terms while the spectrum is also modified and shifted by the AC terms. The resultant normalized envelope is a summation of all the DC and AC components.

If the input signal is a CW signal, then there are basically three groups of terms inside the braces; DC terms, fundamental baseband signal frequency terms and second harmonic baseband signal frequency terms. The DC terms are functions of the amplitude imbalance and DC offsets, independent of phase imbalance. A DC offset introduces a fundamental harmonic frequency which has the same frequency as the baseband signal. Other errors only affect the magnitude of these ripples. Without DC offsets, ripples of the fundamental frequency disappear completely. Ripples with a second harmonic frequency appear only when there is an amplitude or phase imbalance. When the two channels are matched, all the ripples disappear and the terms inside the braces is unity.

3.2 Phase and Instantaneous Frequency Measurement

Using Eqs.(8) and (9), the phase of the baseband signal is given by

$$\begin{aligned} a(t) &= \tan^{-1}\left[S_q(t)/S_i(t)\right] \\ &= \tan^{-1}\left\{ R\left[\sin[a_o(t)]\cos(\Delta\phi) + \cos[a_o(t)]\sin(\Delta\phi) + a_{qo}/[a(t)K_q/2]\right] \right. \\ &\qquad \left. / \left[\cos[a_o(t)] + a_{io}/[a(t)K_i/2]\right]\right\} \end{aligned} \tag{16}$$

where the argument has also been expressed in terms of relative and normalized parameters. The only exception is that the DC offset $\{a_{qo}/[a(t)K_q/2)]\}$ in the quadrature channel is normalized by the gain in the quadrature channel.

The deviation in measurement from the case of an ideal demodulator is emphasized in this analysis. The phase error is defined by the difference between the measured phase function and the input phase function of the baseband signal as

$$\Delta a(t) = a(t) - a_o(t) \tag{17}$$

For a specific set of imbalances and DC offsets, the phase error can be fully characterized by plotting $\Delta a(t)$ over an input phase change of 2π radians. The measured phase value $[a(t)]$ is then obtained from Eq.(17) once the phase function of the input signal is known. If the input signal is a CW signal, the phase is linearly proportional to time and an input phase change of 2π radians simply corresponds to one period of the signal. It is to be noted that the imbalances and DC offsets are usually a function of frequency.

The measured instantaneous frequency deviation from the input baseband signal is then obtained by differentiating Eq.(17) with respect to time. Hence,

$$\frac{\partial[\Delta a(t)]}{\partial t} = \frac{\partial[\Delta a(t)]}{\partial[a_o(t)]} \frac{\partial[a_o(t)]}{\partial t} \tag{18}$$

where $\partial[\Delta a(t)]/\partial[a_o(t)]$ is the partial derivative of the measured phase change with respect to the input phase and is dimensionless. It is also a very useful parameter in characterizing the instantaneous frequency deviation due to the imbalances and DC offsets. This parameter is referred to as the normalized instantaneous frequency deviation in this report. By substituting Eq. (16) into Eq.(17) and taking the partial derivative with respect to the input phase, the general expression for the normalized instantaneous frequency deviation can be shown as

$$\frac{\partial[\Delta a(t)]}{\partial[a_o(t)]} = R\left[\cos(\Delta\phi) + \sin[a_o(t)]\, a_{qo}/[a(t)K_q/2] + \cos[a_o(t) + \Delta\phi]\, a_{io}/[a(t)K_i/2]\right]$$
$$/\left\{\left[\cos[a_o(t)] + a_{io}/[a(t)K_i/2]\right]^2 + R^2\left[\sin[a_o(t) + \Delta\phi] + a_{qo}/[a(t)K_q/2]\right]^2\right\} - 1 \tag{19}$$

For a given set of imbalances and DC offsets, the normalized frequency deviation is completely determined by a plot of $\partial[\Delta a(t)]/\partial[a_o(t)]$ over an input phase change of 2π radians. The measured frequency deviation from the input signal is determined by multiplying the normalized frequency deviations by the instantaneous frequency of the input signal at the baseband frequency as given in Eq.(18). If the imbalances and DC offsets are about the same, independent of IF frequency, the measured frequency error due to the ripples can be minimized by choosing an IF signal which gives the lowest baseband frequency.

4.0 AMPLITUDE AND PHASE IMBALANCES ONLY

When there are only amplitude and phase imbalances between the in–phase and quadrature channels, the instantaneous power of the envelope of the baseband signal [Eq.(10)], can be simplified to

$$S_i^2(t) + S_q^2(t) = [a(t)K_i]^2/4 \left\{ 1/2 + R^2/2 + 1/2 \cos[2a_o(t)] - R^2/2 \cos\{2[a_o(t) + \Delta\phi]\} \right\} \quad (20)$$

Inside the braces, there are DC and AC ripple terms, with the latter having a frequency twice that of the baseband frequency. Rewriting the AC ripple terms separately, we have

$$\text{Ripple} = 1/2 \cos[2a_o(t)] - R^2/2 \cos\{2[a_o(t) + \Delta\phi]\} \quad (21)$$

The locations of the peak and null of the ripples can be found by taking the derivative of Eq.(21) with respect to $a_o(t)$ and equating the result to zero. Therefore,

$$a_o(t) = [\tan^{-1}(1/A)]/2 \quad \text{or}$$
$$= \left[\cos^{-1}[\, A \,/\, (\, 1 + A^2\,)^{1/2}]\right]/2 \quad (22)$$

where $$A = \left[\, 1 - R^2 \cos(2\,\Delta\phi\,)\right] / \left[\, R^2 \sin(2\,\Delta\phi\,)\right] \quad (23)$$

The location of the peak or null depends on the sign of A. The peak and null locations are separated by 180 degrees. Inserting Eq.(22) into Eq.(21) and making use of Eq.(23), the value of the peak or null ripple is reduced to

$$\text{Peak or Null Ripple} = \left[\, 1 + R^4 - 2\, R^2 \cos(2\,\Delta\phi)\right]^{1/2} / \, 2 \quad (24)$$

The shape of the envelope is distorted by the ripples and the magnitude of the ripples is a function of both the amplitude and phase imbalances. The mean of the ripples is zero and since the magnitude of the peak equals the null, the peak–to–peak variation of the ripples is simply twice of that given in Eq.(24). The mean of the envelope [Eq.(20)] is $1/2 + R^2/2$ which is only a function of the amplitude imbalance. In practice, the amplitude imbalance is small and R is close to unity. As a result, the mean of the undistorted envelope is only slightly affected. Therefore, the ratio of the peak–to–peak variation of the ripples to the mean of the envelope is given by

Peak–to–peak Ripple/mean

$$= \left|2\left[\, 1 + R^4 - 2\, R^2 \cos(2\Delta\phi)\right]^{1/2}\right| \, / \, (1 + R^2) \quad (25)$$

This simple ratio gives a relative measure on the AC ripple distortion introduced by the imbalances on the signal envelope and can be measured readily. When R is replaced by 1/R or when R is expressed in terms of ± dB, the ratio of the peak–to–peak ripple to the mean remains the same. This ratio is also symmetrical with respect to the phase imbalance as indicated by the cosine function. This is expected because the magnitude of the systematic errors should be independent of the choice of the reference channel. A plot of the ratio of the peak–to–peak ripple to mean is plotted in Fig.2 as a function of amplitude

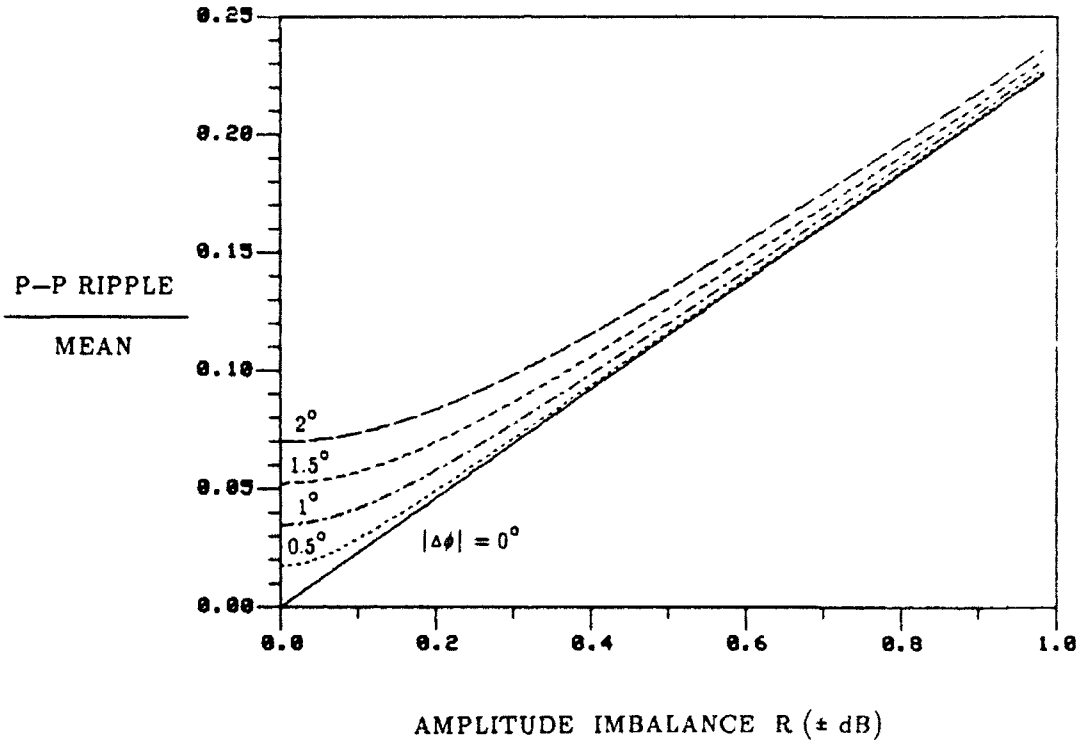

Figure 2 Normalized Peak–to–peak Ripple Versus Amplitude and Phase Imbalances

and phase imbalances. For $\Delta\phi$ small and as R gets larger, the ratio will eventually approach the maximum limit of 2.

The RMS value of the ripples to the mean can also be obtained directly by using the simple fact that for a sinusoidal wave, the RMS value is simply equal to the peak value divided by the square root of 2.

When there are only imbalances present in the I/Q demodulator, the phase error as defined by Eq.(17) can be simplified to

$$\Delta a(t) = \tan^{-1}\left[R\cos(\Delta\phi)\,\{\tan[a_o(t)] + \tan(\Delta\phi)\}\right] - a_o(t) \qquad (26)$$

The argument is characterized by an offset $[\tan(\Delta\phi)]$ and a scaling factor $[R\cos(\Delta\phi)]$. When $a_o(t)$ equals $-\Delta\phi$, the phase error is $\Delta\phi$.

The locations of the zero–crossings in the principal branch $\left[\,|a_o(t)| \le 90^\circ\right]$ is obtained by setting Eq.(26) to zero and then solving for $[a_o(t)]$ to yield

$$[a_o(t)] = \tan^{-1}\left[R\sin(\Delta\phi)/\,[1 - R\cos(\Delta\phi)]\right] \qquad (27)$$

For $R\cos(\Delta\phi) \neq 1$, one of the zero–crossings is located in the range of $\left|a_o(t)\right| < 90^\circ$. The other zero–crossings can also be found directly from Eq.(26) by letting $a_o(t) = \pm 90^\circ$ for $R\cos(\Delta\phi) \neq 0$.

Because the tangent function is periodic and if there are three zero–crossings over the range of 180 degrees, the period of the phase error as a function of $a_o(t)$ must be half that of the input phase cycle. As a result, for a sinusoidal input signal the phase error introduced by the imbalances is not purely sinusoidal, but with a fundamental frequency component which is twice that of the input baseband frequency.

For $R\cos(\Delta\phi) = 1$, the zero–crossings are located only at $a_o(t) = \pm 90^\circ$. The phase error is of the same sign of the phase imbalance and the period of the phase error as a function of $a_o(t)$ is also half that of the input phase cycle.

The normalized instantaneous frequency deviation as given by Eq.(19) can be simplified to

$$\partial[\Delta a(t)]/\partial[a_o(t)] = R\cos(\Delta\phi)/\left[\cos^2[a_o(t)] + R^2\sin^2[a_o(t) + \Delta\phi]\right] - 1 \qquad (28)$$

The maximum and minimum locations of the phase error are obtained by setting the derivative [Eq.(28)] to zero. Hence,

$$\tan^2[a_o(t)]\Big[\, R\cos(\Delta\phi) - R^2\cos^2(\Delta\phi)\Big]$$
$$-\tan[a_o(t)]\Big[\, 2\,R^2\cos(\Delta\phi)\sin(\Delta\phi)\Big] + R\cos(\Delta\phi) - 1 - R^2\sin^2(\Delta\phi) = 0 \qquad (29)$$

which is of quadratic form and the solutions can be found readily. Since the period of the phase error is half that of the input phase cycle, one solution is the maximum location while the other is the minimum.

Since the phase error distribution is no longer purely sinusoidal over an input phase change of 2π radians, its characteristics are more suitably described by the RMS, mean and peak–to–peak parameters. The three parameters of the phase error as a function of amplitude and phase imbalances are plotted in Figs. 3(a) to 3(c). The RMS and peak–to–peak values are only a function of the absolute value of the phase imbalance because the sign of the phase imbalance only changes the sign of the offset, not the scaling factor in Eq.(26). When R is expressed in dB, the peak–to–peak value is also symmetrical to R = 0 because when R is replaced by 1/R, the offset will be changed, but the arctangent function is replaced by its cotangent function. This will only change the shape of the phase error, not its peak–to–peak value and the mean error is no longer zero. As expected, the ratio of the RMS value to its peak–to–peak value is no longer equal to $1/(2^{3/2})$ as for a sinusoidal wave.

The locations of the maximum and minimum instantaneous frequency deviations are found by differentiating Eq.(28) with respect to $a_o(t)$ and equating the result to zero. Hence

$$\partial^2[\Delta a(t)]/\partial^2[a_o(t)] = R\cos(\Delta\phi)\Big[2\cos[a_o(t)]\sin[a_o(t)] - 2R^2\sin[a_o(t)+\Delta\phi]$$
$$\cdot\cos[a_o(t)+\Delta\phi]\Big]/\Big[\cos^2[a_o(t)] + R^2\sin^2[a_o(t)+\Delta\phi]\Big]^2 = 0 \qquad (30)$$

Therefore

$$a_o(t) = \tan^{-1}\Big[\, R^2\sin(2\Delta\phi)/\,[\,1 - R^2\cos^2(2\Delta\phi)]\Big]/2 \qquad (31)$$

There are two solutions for the arctangent function over the 360–degree range. After dividing by two, one will provide the maximum location and the other the minimum within the 180–degree range.

As can be seen from Eq.(28), the relative shape of the normalized instantaneous frequency deviation is only a function of the absolute phase imbalance because $\cos(\Delta\phi)$ is an even function of $\Delta\phi$. Moreover when R is replaced by 1/R, the relative shape is also not affected. However, the position of the normalized instantaneous frequency deviation as a function of $a_o(t)$ is a function of both the imbalances. When $R \neq 1$ and $\Delta\phi \neq 0$, the period of the normalized instantaneous frequency deviation as a function of $a_o(t)$ is also half that of

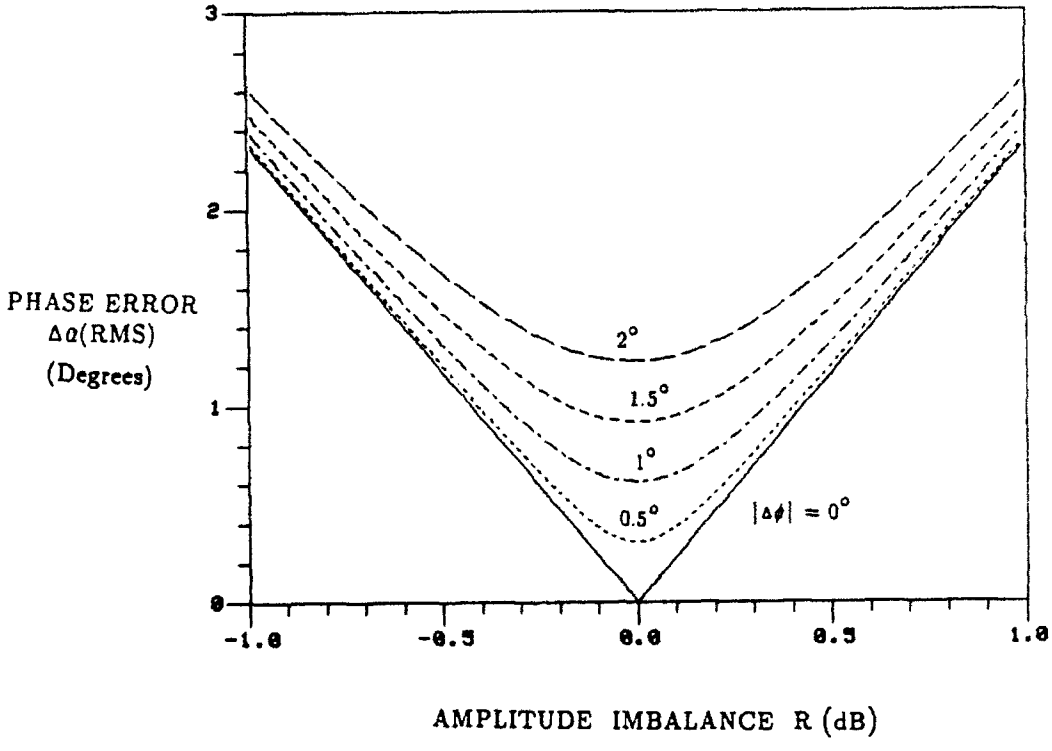

(a) RMS

Figure 3 Phase Error Versus Amplitude and Phase Imbalances

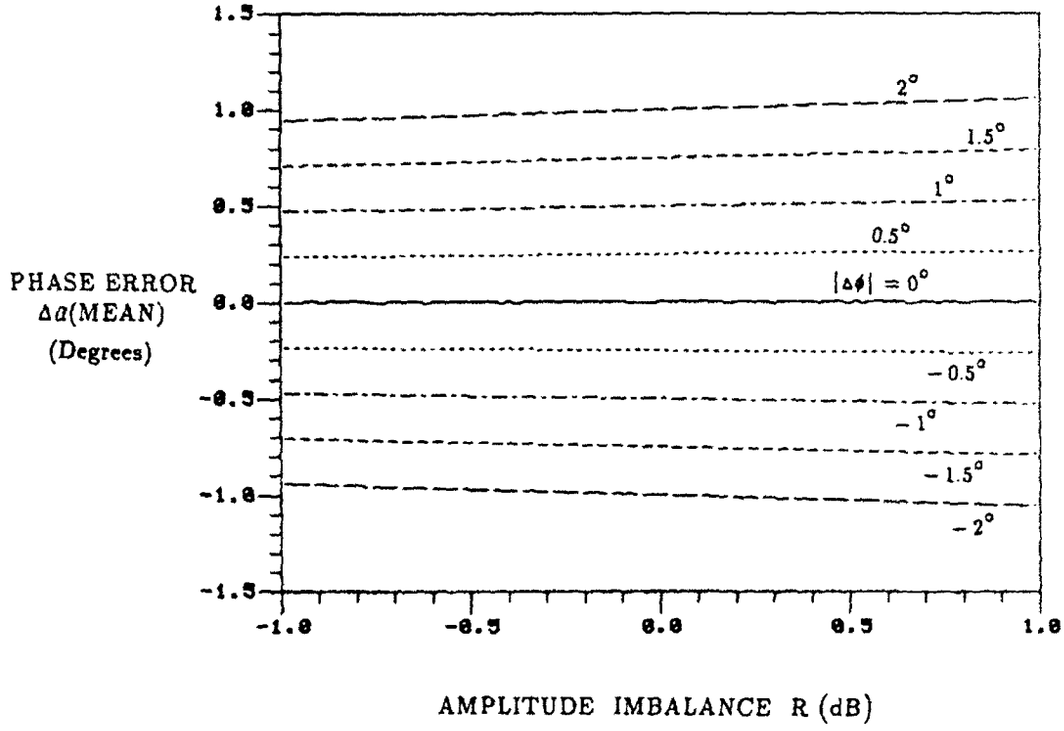

(b) Mean

Figure 3 Phase Error Versus Amplitude and Phase Imbalances

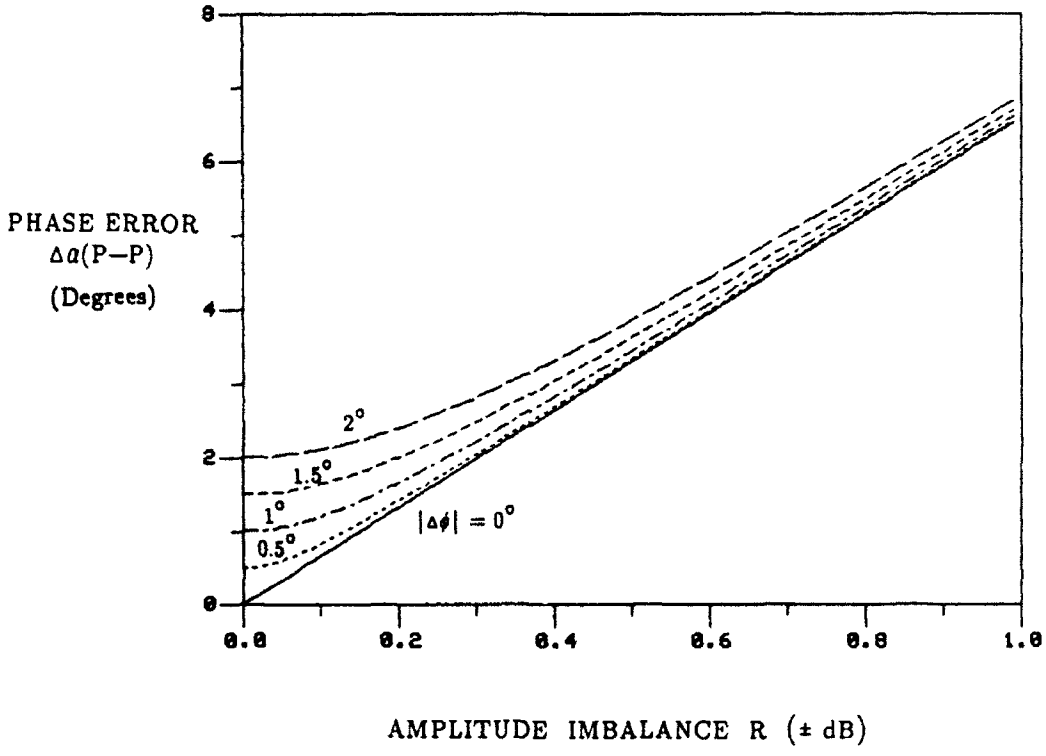

(c) Peak–to–peak

Figure 3 Phase Error Versus Amplitude and Phase Imbalances

the input phase cycle. This period is generated by the squared terms of both the cosine and sine functions. Since the denominator is always positive, the sign of the first term of Eq.(28) is completely determined by $\cos(\Delta\phi)$. For $\cos(\Delta\phi) \geq 0$ or $(\Delta\phi) \leq 90$ degrees, $\partial[\Delta a(t)]/\partial[a_o(t)] \geq -1$. For $\cos(\Delta\phi) \leq 0$ or $180 \geq (\Delta\phi) \geq 90$ degrees, $\partial[\Delta a(t)]/\partial[a_o(t)] \leq -1$.

The peak–to–peak normalized instantaneous frequency deviation is plotted in Fig. 4 as a function of the imbalances. The ratio of the RMS value to its peak–to–peak value is approximately equal to $1/(2^{3/2})$ when the imbalances are small. However, the normalized instantaneous frequency deviation as a function of $a_o(t)$ is not sinusoidal over an input phase change of 2π radians, and the positive portion is higher in magnitude than the negative one. In addition, the mean of the normalized instantaneous frequency deviation is always equal to zero.

4.1 Amplitude Imbalance Only $(\Delta\phi = 0)$

With amplitude imbalance only, the power of the envelope as given in Eq.(20) can be simplified further to

$$S_i^2(t) + S_q^2(t) = [a(t)K_i]^2/4 \left\{ [1/2 + R^2/2] + [1/2 - R^2/2] \cos[2\, a_o(t)] \right\} \tag{32}$$

Similar to the general case where there are both amplitude and phase imbalances, there are also DC terms and AC ripple terms which are of twice the baseband signal frequency. The peak–to–peak ripple is simply given by $|1 - R^2|$. The ratio of the peak–to–peak ripple to mean of the envelope is then given by

$$\text{Peak–to–peak ripple/mean} = 2 \left| 1 - R^2 \right| / \left[1 + R^2 \right] \tag{33}$$

This special case is illustrated in Fig. 2 by the solid curve. For R close to unity, the ratio of the peak–to–peak ripple/mean can be shown to be approximately given by $|2\Delta R|$, where $R = 1 + \Delta R$. Therefore, when the ratio is plotted as a function of R and expressed in dB, it is approximately a straight line with intercept point at the origin as shown. When R is close to unity, the plot is near the origin along the horizontal axis because R is plotted in logarithmic scale.

The measured phase error as given by Eq.(26) can be simplified further to

$$\Delta a(t) = \tan^{-1}\left[R \tan[a_o(t)] \right] - a_o(t) \tag{34}$$

Following a similar procedure as given in Section 4.0, the locations of the zero–crossing points are at

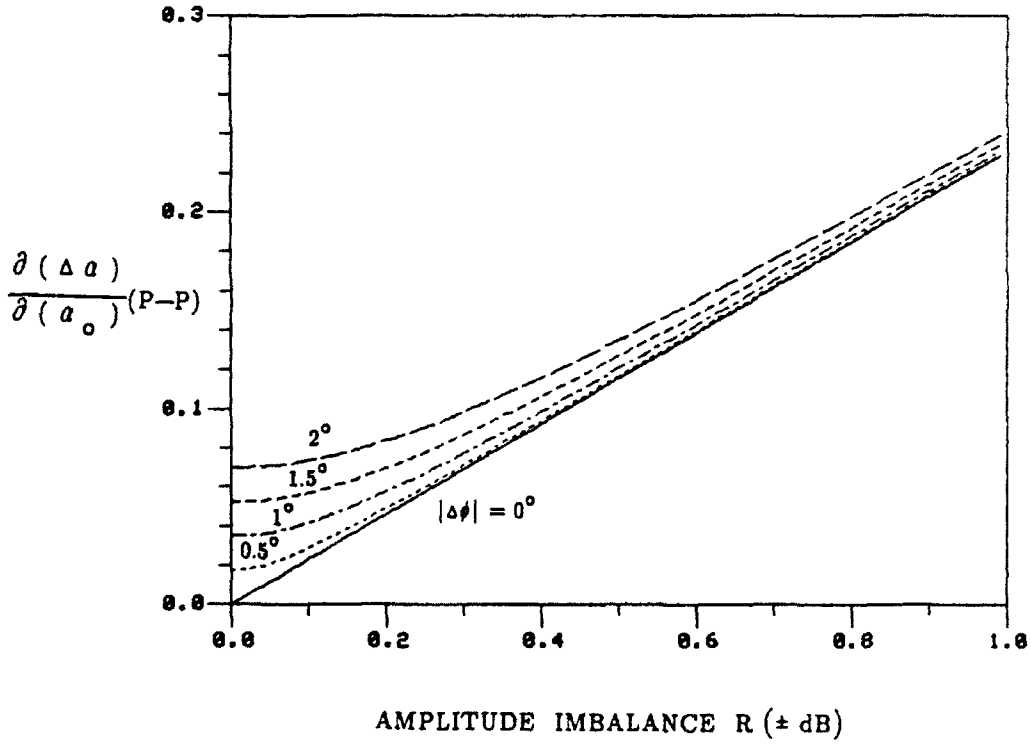

Figure 4 Normalized Peak–to–peak Instantaneous Frequency Deviation Versus Amplitude and Phase Imbalances

$$a_o(t) = 0 \text{ and } \pm 90^o \text{ , for } R \neq 1 \tag{35}$$

As a result when there is an imbalance in amplitude ($R \neq 1$), there are three crossing points over an input phase change of 180 degrees. In other words, the ripple of the phase error is periodic with a period equal to one half of the period of the input baseband signal.

The normalized instantaneous frequency deviation as given by Eq.(28) can be simplified further to

$$\partial[\Delta a(t)]/\partial[a_o(t)] = R \Big/ \Big[\cos^2[a_o(t)] + R^2 \sin^2[a_o(t)] \Big] - 1 \tag{36}$$

and similarly, the locations of the maximum and minimum phase errors are given by

$$[a_o(t)] = \tan^{-1}\Big[\pm 1/\sqrt{R} \Big] \tag{37}$$

To verify whether it is a maximum or minimum, another derivative is taken to determine its sign. If the second derivative is negative, it is the maximum location, otherwise it is the minimum. For $R > 1$, the maximum phase error occurs when $\tan[a_o(t)] = 1/\sqrt{R}$, and the minimum phase error occurs when $\tan[a_o(t)] = -1/\sqrt{R}$. For $R < 1$, it is the other way around.

For $R > 1$, the maximum phase error is obtained by substituting $a_o(t)$ back into Eq. (34) and yields

$$\Delta a(t)_{max} = \tan^{-1}\Big[\sqrt{R}\Big] - \tan^{-1}\Big[1/\sqrt{R} \Big] \tag{38}$$

Similarly, the magnitude of the minimum phase error is found to be the same as the maximum. As a result, the phase error distribution is periodic and symmetrical. The peak–to–peak phase error is simply twice that of Eq.(38) and is shown by the solid line in Fig.3(c). For $R < 1$, the maximum phase error is identical to Eq.(38) when R is replaced by $1/R$.

The locations of the maximum and minimum normalized instantaneous frequency deviations are found from Eq.(31) to be at $[2a_o(t)] = 0$, and $\pm \pi$, for $R \neq 1$ or at $a_o(t) = 0$, and $\pm \pi/2$. Substituting the locations back into Eq.(37), the maximum and minimum of the normalized instantaneous frequency deviation are $R - 1$, at $a_o(t) = 0$ and $1/R - 1$ at $a_o(t) = \pm \pi/2$ respectively. For $R > 1$, $R - 1$ is the maximum, and $1/R - 1$ is the minimum. For $R < 1$, $1/R - 1$ is the maximum, and $R - 1$ is the minimum. As a result, when R is replaced by $1/R$, the maximum and minimum deviations are the same. The peak–to–peak normalized instantaneous frequency deviation is shown by the solid line in Fig.4. It is to be noted that the absolute maximum is larger than the absolute minimum. In addition, there is no upper bound as R approaches either 0 or infinity, but there is a lower bound.

4.2 Phase Imbalance Only (R = 1)

When there is phase imbalance only, Eq.(20) is reduced further to

$$S_i^2(t) + S_q^2(t) = [a(t)K_i]^2/4 \left\{ 1 + \sin(\Delta\phi) \sin [2a_o(t) + \Delta\phi] \right\} \tag{39}$$

As in the case of amplitude imbalance only, there is a DC term as well as a second harmonic baseband frequency term. The ratio of the peak–to–peak ripple to mean is simply given by

$$\text{Peak–to–peak/mean} = \left| 2 \sin(\Delta\phi) \right| \tag{40}$$

Eq.(40) is plotted in Fig. 2 for $|\Delta\phi| = 0^\circ$, 0.5°, 1.0°, 1.5° and 2.0° at R = 0 dB. For small $\Delta\phi$, the peak–to–peak/mean ratio is approximately twice the phase imbalance.

The phase error as given by Eq.(26) can be simplified further to

$$\Delta a(t) = \tan^{-1}\left[\cos(\Delta\phi) \{\tan[a_o(t)] + \tan(\Delta\phi)\} \right] - a_o(t) \tag{41}$$

Now the argument is also scaled by a scaling factor equal to $\cos(\Delta\phi)$ which is different from the amplitude imbalance case in two aspects; it is bipolar and is less than unity. In addition, there is also an offset given by $\tan(\Delta\phi)$.

The location of the zero–crossing is obtained by setting Eq.(41) to zero and yields

$$\begin{aligned} a_o(t) &= [90^\circ - \Delta\phi/2] \quad \text{for} \quad \Delta\phi/2 \geq 0 \quad \text{and} \\ &= [-90^\circ + \Delta\phi/2] \quad \text{for} \quad \Delta\phi/2 \leq 0 \end{aligned} \tag{42}$$

Similar to the last two cases, the other two zero–crossing points are located at $a_o(t) = \pm 90^\circ$.

The normalized instantaneous frequency deviation as given by Eq.(28) can be simplified further to

$$\partial[\Delta a(t)]/\partial[a_o(t)] = \cos(\Delta\phi)/\left[\cos^2[a_o(t)] + \sin^2[a_o(t) + \Delta\phi] \right] - 1 \tag{43}$$

The locations of the maximum and minimum phase errors are determined by equating Eq.(43) to zero and solving for the value of $a_o(t)$. The maximum and minimum phase errors can then be shown as

$$\Delta a(t) = \tan^{-1}\left[\left[\sin(\Delta\phi) \pm \sqrt{2\cos(\Delta\phi)\{1-\cos(\Delta\phi)\}}\right] / \left[1-\cos(\Delta\phi)\right]\right]$$
$$-\tan^{-1}\left[\left[\cos(\Delta\phi)\sin(\Delta\phi) \pm \sqrt{2\cos(\Delta\phi)\{1-\cos(\Delta\phi)\}}\right] / \left[\cos(\Delta\phi)-\cos^2(\Delta\phi)\right]\right] \quad (44)$$

The minimum error occurs when the sign in front of the square root is positive while for the maximum error, the sign is negative. The magnitude of one error is much larger than the other. The larger error is determined by the sign of the phase imbalance. If the phase imbalance is positive, the maximum error is larger than the minimum. For small phase imbalance, the peak–to–peak error is slightly larger than the input phase imbalance. This difference is bigger for larger phase imbalances. The RMS, mean and peak–to–peak phase errors are plotted in Fig. 3(a), 3(b) and 3(c) respectively versus phase imbalance at $|\Delta\phi| = 0^\circ, 0.5^\circ, 1.0^\circ, 1.5^\circ$ and 2.0° .

The maximum and minimum locations of the normalized instantaneous frequency deviation are found by differentiating Eq.(43) with respect to $a_o(t)$ and equating the result to zero. After some manipulation, the maximum and minimum locations are found to be

$$a_o(t) = \pm\,\pi/4 - \Delta\phi/2 \quad (45)$$

Substituting Eq.(45) into Eq.(43) and simplifying, the maximum and minimum normalized instantaneous frequency deviations are

$$\partial[\Delta a(t)]/\partial[a_o(t)] = \cos(\Delta\phi)\left\{1 + \left[\left[-\sin(\Delta\phi) \pm 1\right]/\cos(\Delta\phi)\right]^2\right\}/2 - 1 \quad (46)$$

For small phase imbalance ($|\Delta\phi| \leq 90^\circ$), the numerator is always positive. The maximum normalized instantaneous frequency deviation occurs when the absolute value of $[-\sin(\Delta\phi) \pm 1]$ is maximum, i.e. when $(\Delta\phi)$ is positive, then -1 is chosen. When $(\Delta\phi)$ is negative, then $+1$ is chosen. If $(\Delta\phi)$ is negative, the reverse is true.

The peak–to–peak normalized instantaneous frequency deviation is plotted in Fig.4 versus $|\Delta\phi| = 0^\circ, 0.5^\circ, 1.0^\circ, 1.5^\circ$ and 2.0°.

5.0 DC OFFSETS ONLY (R = 1 and $\Delta\phi = 0$)

With only DC offsets, Eq.(10) can be simplified to

$$S_i^2(t) + S_q^2(t) = [a(t)\,K_i]^2/4 \left\{ 1 + \{a_{io}/[a(t)K_i/2]\}^2 + \{a_{qo}/[a(t)K_i/2]\}^2 + 2\,a_{io}/[a(t)K_i/2]\,\cos[a_o(t)] + 2\,a_{qo}/[a(t)K_i/2]\,\sin[a_o(t)] \right\} \tag{47}$$

For a CW signal, the terms inside the braces are simply DC terms and fundamental baseband frequency terms. The peak or null occurs at

$$[a_o(t)]_{\text{peak or null}} = \cos^{-1}\left[[a^2_{io}/\,(a^2_{io} + a^2_{qo})]^{1/2} \right] \tag{48}$$

and the peak–to–peak ripple/mean ratio can be shown to be

$$\text{Peak–to–peak ripple/mean} = 4 \left[(a^2_{io} + a^2_{qo})/[a(t)K_i/2]^2 \right]^{1/2} \Big/ \left[1 + \{a_{io}/[a(t)K_i/2]\}^2 + \{a_{qo}/[a(t)K_i/2]\}^2 \right] \tag{49}$$

The normalized peak ripple is only a function of the absolute value of the normalized offsets and is plotted in Fig. 5. For small normalized offsets, the ratio is approximately proportional to four times the normalized offsets added on a RMS basis.

From Eqs. (16) and (17), the phase error as a function of DC offsets only is simplified to

$$\Delta a(t) = \tan^{-1}\left\{ \left[\sin[a_o(t)] + a_{qo}/[a(t)K_q/2] \right] \Big/ \left[\cos[a_o(t)] + a_{io}/[a(t)K_i/2] \right] \right\} - a_o(t) \tag{50}$$

The normalized instantaneous frequency deviation given in Eq.(19) can be simplified further to

$$\partial[\Delta a(t)]/\partial[a_o(t)] = \left[1 + \sin[a_o(t)]\,a_{qo}/[a(t)K_q/2] + \cos[a_o(t)]\,a_{io}/[a(t)K_i/2] \right] \Big/ \left\{ 1 + \left[a_{qo}/[a(t)K_q/2] \right]^2 + \left[a_{io}/[a(t)K_i/2] \right]^2 + 2\,\sin[a_o(t)]\,a_{qo}/[a(t)K_q/2] + 2\,\cos[a_o(t)]\,a_{io}/[a(t)K_i/2] \right\} - 1 \tag{51}$$

The maximum and minimum phase errors are obtained by setting Eq.(51) to zero and yields

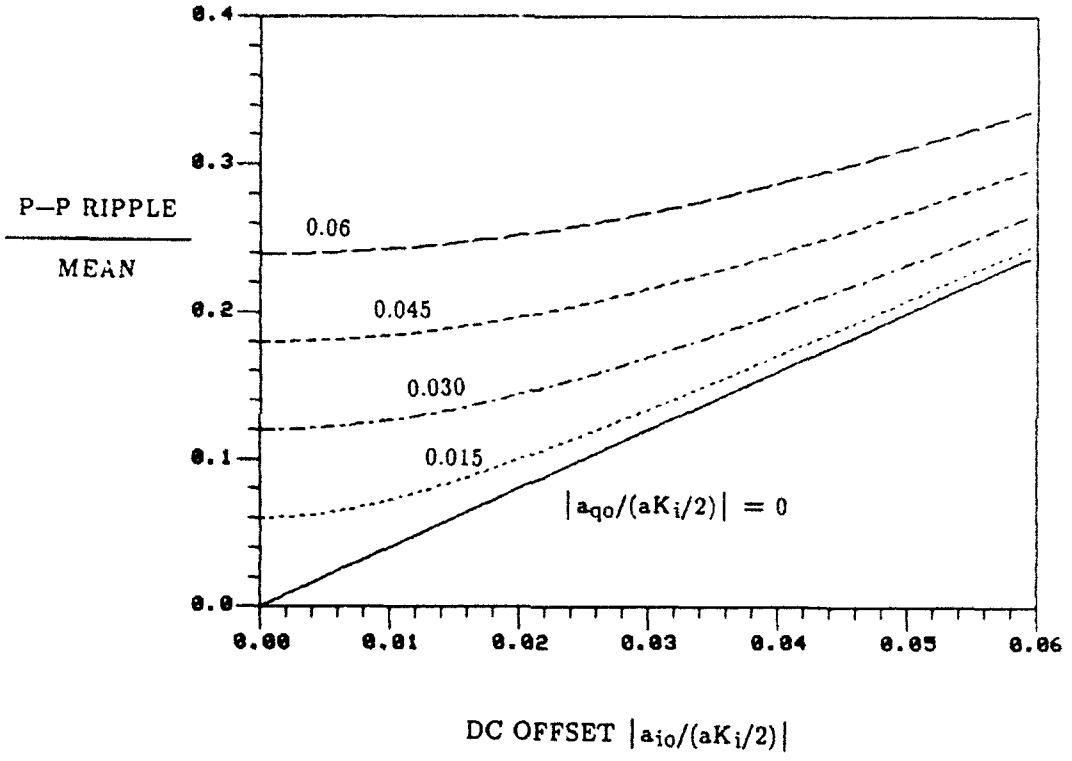

Figure 5 Normalized Peak–to–peak Ripple Versus DC Offsets

$$\left[a_{io}/[a(t)K_i/2]\right]^2 + \left[a_{qo}/[a(t)K_q/2]\right]^2 + \cos[a_o(t)]\ a_{io}/[a(t)K_i/2]$$
$$+ \sin[a_o(t)]\ a_{qo}/[a(t)K_i/2] = 0 \qquad (52)$$

After rearranging and squaring, we have

$$\cos^2[a_o(t)]\left\{\left[a_{qo}/[a(t)K_q/2]\right]^2 + \left[a_{io}/[a(t)K_i/2]\right]^2\right\} + \cos[a_o(t)]\ 2a_{io}/[a(t)K_i/2]$$
$$\cdot\left\{\left[a_{io}/[a(t)K_i/2]\right]^2 + \left[a_{qo}/[a(t)K_q/2]\right]^2\right\}$$
$$+\left\{\left[a_{io}/[a(t)K_i/2]\right]^2 + \left[a_{qo}/[a(t)K_q/2]\right]^2\right\}^2 - \left[a_{qo}/[a(t)K_i/2]\right]^2 = 0 \qquad (53)$$

Now Eq.(53) is in quadratic form and the solution can be obtained readily. One solution will give the location of the minimum while the other will give the maximum. From Eq.(50), if the sign of the DC offset is reversed, the location of $a_o(t) = 0$ will be shifted by the same amount but on the opposite side. This will only change the relative position of the ripples, not its absolute peak amplitude. As a result, the maximum and minimum phase errors are only a function of the magnitude of both the offsets and thus should be independent of the sign of the offset in each channel.

The zero–crossing point is obtained by equating the phase error of Eq.(50) to zero and yields

$$a_o(t) = \tan^{-1}\left[\ (a_{qo}/K_q)\ /(a_{io}/K_i)\right] \qquad (54)$$

There is only one zero–crossing over an input phase change of 180 degrees, and thus the period of the phase error is the same as the input phase cycle.

The mean of the phase error is found to be zero for a signal with a constant envelope and over an input phase change of 2π radians. The peak–to–peak phase error as a function of DC offsets is plotted in Fig. 6. For small DC offsets, the phase error is approximately sinusoidal in shape and the ratio of the RMS value to its peak–to–peak value is approximately equal to $1/(2^{3/2})$. As the DC offsets get bigger, the maximum positive phase error is no longer equal to the maximum negative one. However the ratio of the RMS value to its peak–to–peak value remains approximately equals to $1/(2^{3/2})$.

The location of the maximum or minimum normalized instantaneous frequency deviation is determined by taking another derivative of Eq.(50) with respect to the input phase and equating the result to zero. The solution is found to be the same as given in Eq.(54). As a result, the maximum and minimum locations coincide with the zero–crossing points. From Eq.(54), we have

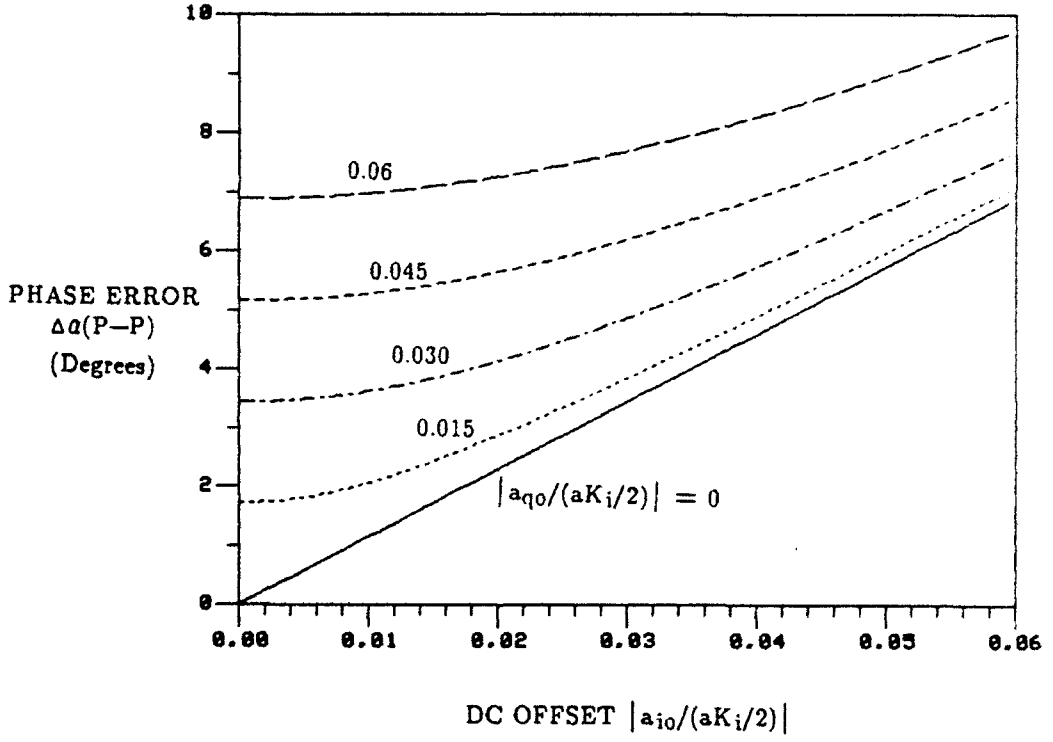

Figure 6 Peak–to–peak Phase Error Versus DC Offsets

$$\sin[a_o(t)] = (a_{qo}/K_q)/\left[(a_{io}/K_i)^2 + (a_{qo}/K_q)^2\right]^{1/2} \quad (55)$$

and

$$\cos[a_o(t)] = (a_{io}/K_i)/\left[(a_{io}/K_i)^2 + (a_{qo}/K_q)^2\right]^{1/2} \quad (56)$$

The maximum or minimum normalized instantaneous frequency deviation is obtained by substituting Eqs.(55) and (56) into Eq.(51). The resultant value is found to be only a function of the square of the DC offsets. Therefore, the maximum and minimum deviations are only a function of the absolute magnitude of the DC offsets.

The mean of the normalized instantaneous frequency deviation is also found to be zero for a signal with a constant envelope and over an input phase change of 2π radians. The RMS of the normalized instantaneous frequency deviation as a function of DC offsets is plotted in Fig. 7. For small DC offsets, the normalized instantaneous frequency deviation is also approximately sinusoidal in shape and the ratio of the RMS value to its peak–to–peak value is approximately equal to $1/(2^{3/2})$. However, the positive and negative halves are not as symmetrical with respect to the zero axis as for the phase error. This non–symmetry is more pronounced for larger DC offsets.

6.0 AMPLITUDE IMBALANCE AND DC OFFSET ONLY

In this special case, we let $a_{qo} = 0$ and $\Delta\phi = 0$.

With only the amplitude imbalance and in–phase channel DC offset, Eq.(10) can be simplified to

$$S_i^2(t) + S_q^2(t) = [a(t)K_i]^2/4 \left\{\left[1/2 + \{a_{io}/[a(t)K_i/2]\}^2 + R^2/2\right] + \cos[a_o(t)]\ 2\ a_{io}/[a(t)K_i/2] + \left[\ 1/2 \cos\ [2a_o(t)] - R^2/2 \cos\ [2a_o(t)]\ \right]\right\} \quad (57)$$

For an input CW signal, the AC ripple terms consist of the fundamental baseband frequency as well as its second harmonic terms. By taking the derivative of the AC ripple terms with respect to $a_o(t)$ and equating the result to zero, the locations of the maximum and minimum are found to be at

$$a_o(t)_{\text{peak or null}} = 0 \text{ and } \pm\pi \quad (58)$$

or

$$a_o(t)_{\text{ peak or null}} = \cos^{-1}\left[\{a_{io}/[a(t)K_i/2]\}/(1 - R^2)\right] \quad (59)$$

By substituting the peak and null locations back into the AC ripple terms, the peak–to–peak value can be found and thus the peak–to–peak/mean ratio can be determined. The AC ripples consist of both the fundamental and second harmonic terms of the baseband frequency. As a result, the peak–to–peak and RMS values are no longer

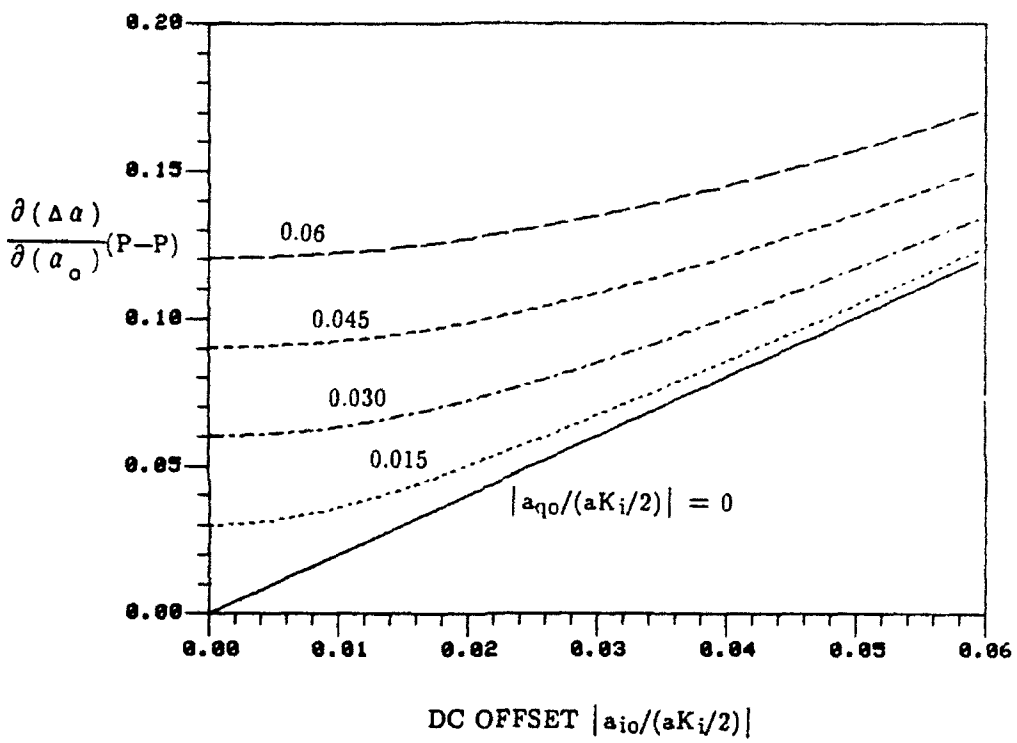

Figure 7 Normalized Peak–to–peak Instantaneous Frequency Deviation Versus DC Offsets

simply related by a constant as in the previous cases. However, the mean value of the ripples is zero, and both the RMS and peak–to–peak values of the ripples are functions of the absolute value of the offset. The peak–to–peak/mean and RMS/mean values are plotted in Figs. 8(a) and (b) respectively as a function of both offset and amplitude imbalance.

Using Eq.(17), the phase error is now simplified to

$$\Delta\alpha(t) = \tan^{-1}\left\{ R \sin[\alpha_o(t)]/\{\cos[\alpha_o(t)] + a_{io}/[a(t)K_i/2]\}\right\} - \alpha_o(t) \qquad (60)$$

Both the locations of the zero crossing and the maximum and minimum phase errors are a function of both the amplitude imbalance and the DC offset. If one mismatch is much greater than the other, we will have one of the special cases analyzed earlier. As can be seen from Eq.(60) if the sign of the DC offset is reversed, only the relative position of the distribution will be affected and both the RMS and peak–to–peak phase errors will remain unchanged. The phase error is zero at $\alpha_o(t) = 0$ and is also of odd symmetry with respect to $\alpha_o(t)$. The RMS and peak–to–peak of the phase errors as a function of both the amplitude imbalance and DC offset are plotted in Figs. 9(a) and (b) respectively. As expected, the ratio of the RMS value to its peak–to–peak value is no longer equal to $1/(2^{3/2})$ as for a sinusoidal wave.

The normalized instantaneous frequency deviation as given by Eq.(19) can now be simplified to

$$\frac{\partial[\Delta\alpha(t)]}{\partial[\alpha_o(t)]} = R\left[1 + \cos[\alpha_o(t)]\, a_{io}/[a(t)K_i/2]\right] / \left\{\{\cos[\alpha_o(t)] + a_{io}/[a(t)K_i/2]\}^2 + R^2 \sin^2[\alpha_o(t)]\right\} - 1 \qquad (61)$$

As can be seen from Eq.(61), since the cosine function is periodic, a change in sign of the DC offset will only change the location of the deviation, not its RMS nor peak–to–peak values. As a result, both the RMS and peak–to–peak phase errors are only a function of the absolute value of the DC offset. The mean value is found to be zero. In addition, because the cosine function is even, the normalized instantaneous frequency deviation is symmetrical with respect to $\alpha_o(t) = 0$. The RMS and peak–to–peak of the normalized instantaneous frequency deviations as a function of both the amplitude imbalance and DC offset are plotted in Figs. 10(a) and (b) respectively.

7.0 EFFECT OF TIME SAMPLING

So far the analysis has been carried out by assuming both the in–phase and quadrature band–limited signals are processed by a continuous–time processor with unlimited processing bandwidth. However, in practice the input signals are sampled, quantized and processed by a discrete–time processor which has a finite bandwidth determined by the Nyquist sampling rate (f_s). In a non–ideal I/Q demodulator where there are imbalances and DC offsets, frequency components higher than those in the

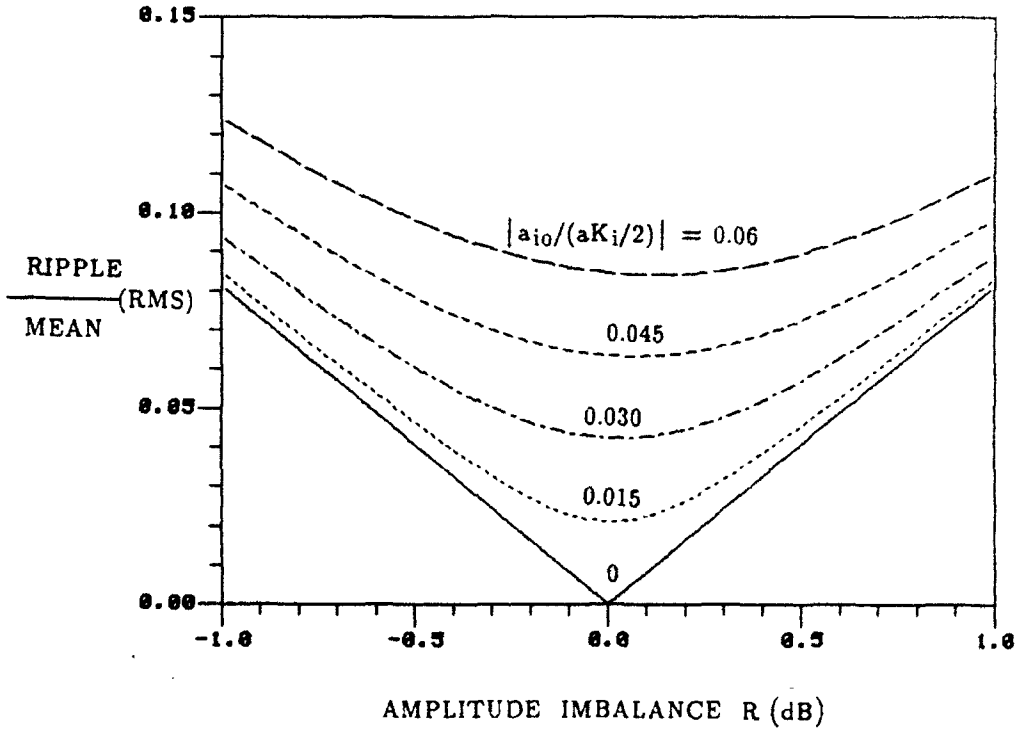

(a) RMS

Figure 8 Normalized Ripple Versus Amplitude Imbalance and DC Offset

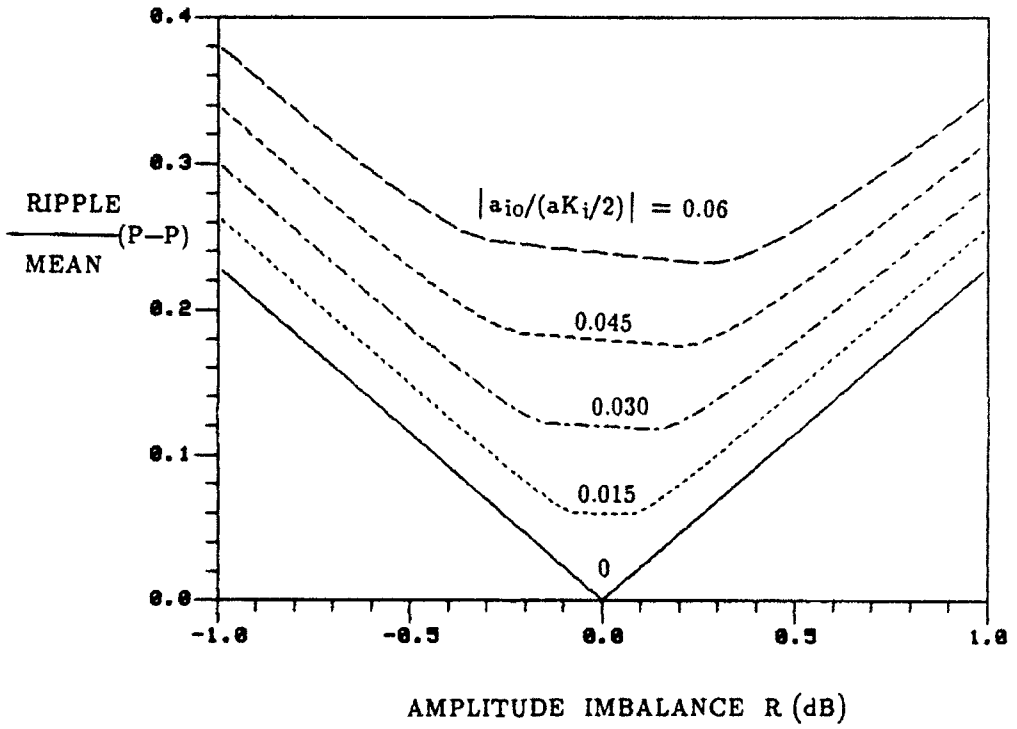

(b) Peak–to–peak

Figure 8 Normalized Ripple Versus Amplitude Imbalance and DC Offset

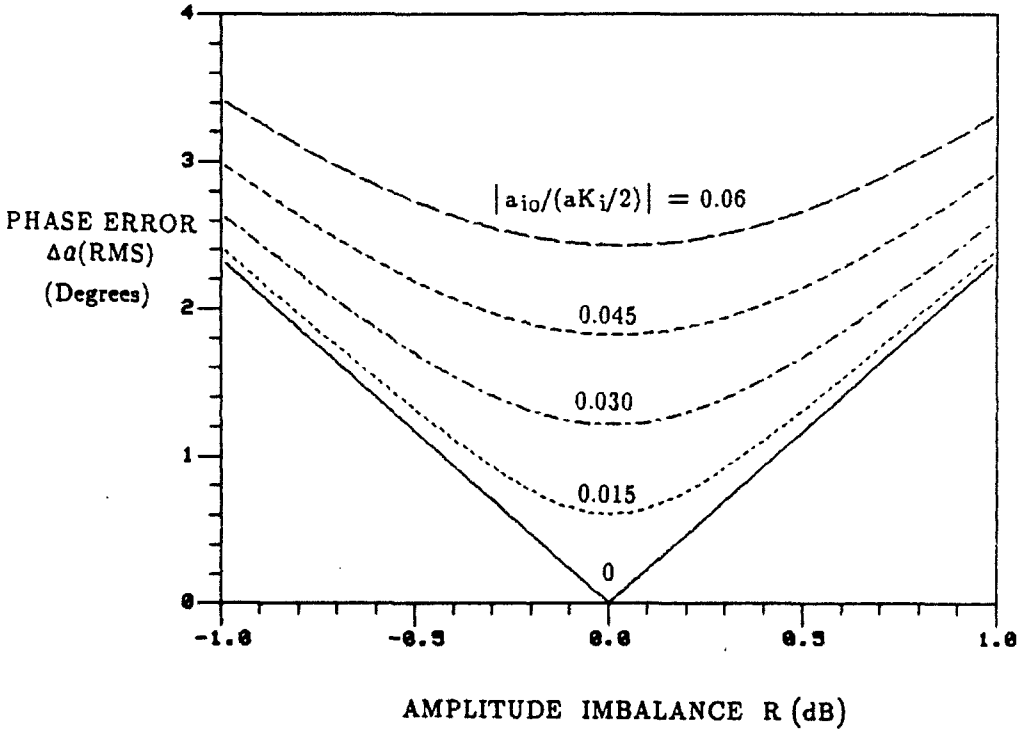

(a) RMS

Figure 9 Phase Error Versus Amplitude Imbalance and DC Offset

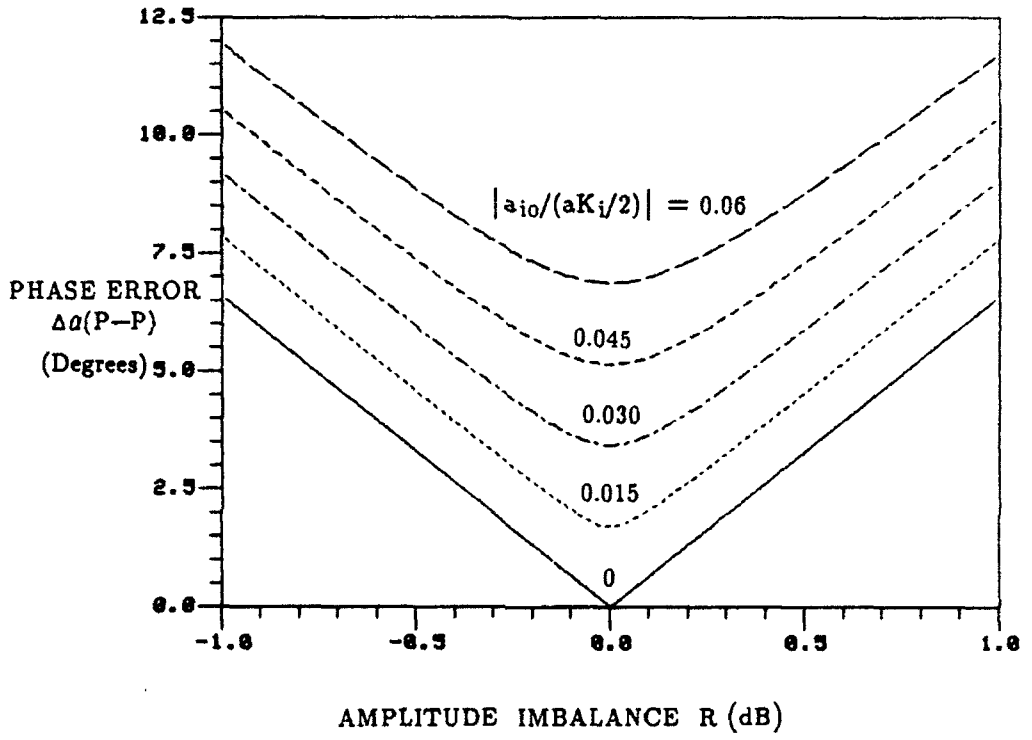

(b) Peak–to–peak

Figure 9 Phase Error Versus Amplitude Imbalance and DC Offset

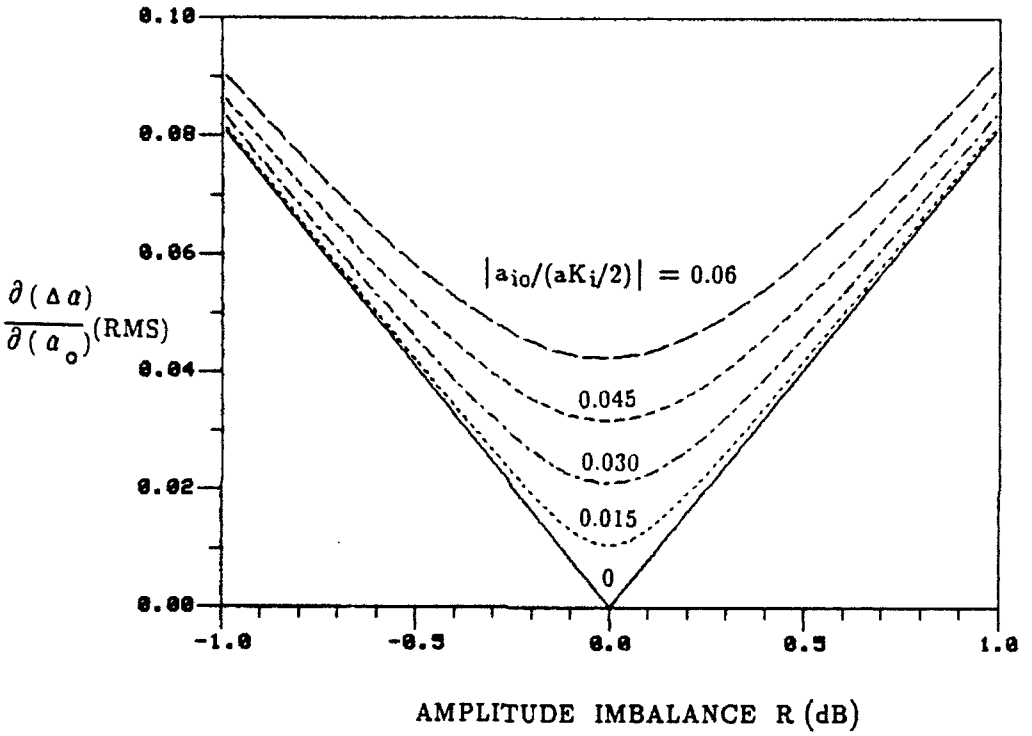

(a) RMS

Figure 10 Normalized Instantaneous Frequency Deviation Versus Amplitude Imbalance and DC Offset

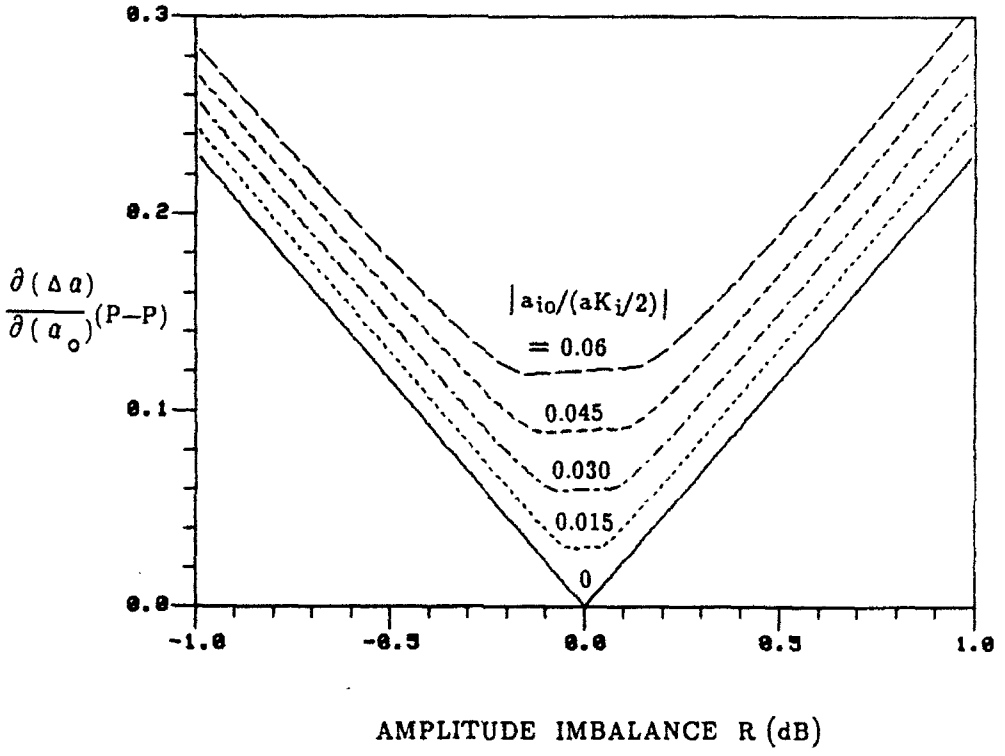

(b) Peak–to–peak

Figure 10 Normalized Instantaneous Frequency Deviation Versus Amplitude Imbalance and DC Offset

band–limited baseband signals can be generated. These higher frequency components are generated by the non–linear operations of computing the power of the envelope and the phase by taking the sum of the squares of the in–phase and quadrature signals and from taking the inverse tangent respectively. As a result, there are differences between the two processors on the demodulated envelope, phase and instantaneous frequency when these higher frequency components are greater than the Nyquist sampling rate.

For a discrete–time processor, the analysis is carried out by replacing the continuous time variable t by its discrete time event t_n. If the maximum frequency of the processed signal is higher than the Nyquist sampling rate, aliasing will occur[13]. The effect due to aliasing can be simply illustrated by considering the case where the input signal is a CW signal and when there are only imbalances in the I/Q demodulator. Eq.(10) shows that there will be ripples introduced on the envelope, which are at twice the frequency of the baseband frequency (f). If 2f is greater than f_s, then aliasing will occur in the discrete–time processor and the frequency of the ripples will have a different component which is the aliased one, given by $(2f - f_s)$.

If the instantaneous frequency of the signal, due to imbalances and DC offsets, is greater than the Nyquist sampling rate, ambiguity can result in the determination of the phase. In other words, the process of phase unwrapping can create errors if the phase difference between consecutive phase points is greater than 180 degrees. When this happens, the computed phase can fall in the wrong principal plane and the resultant instantaneous frequency computed can be seriously affected.

In addition to the ambiguity problem, the instantaneous frequency is also degraded by the problem associated with the approximation used in computing its value. In a discrete–time processor the instantaneous frequency is approximately given by first taking the difference between two contiguous phase samples and then dividing the difference by the sampling interval [Eq.(7)]. This approximation becomes worse as the modulation frequency increases.

In a discrete–time processor, the normalized difference between the measured instantaneous frequency due to imbalances and DC offsets and its input instantaneous frequency is given by

$$\Delta f(t_n)/f_s = \Delta a(t_n)/(2\pi) = \Big\{[a(t_n) - a_o(t_n)] - [a(t_{n-1}) - a_o(t_{n-1})]\Big\}/(2\pi) \tag{62}$$

where the instantaneous frequency deviation has been normalized by the Nyquist sampling frequency. The effect due to aliasing and approximation is a function of input signal frequency, imbalances and DC offsets. Using a CW input signal, a few examples are used to illustrate this effect. The imbalances and DC offsets used are $R = 1.01$, $\Delta\phi = 0.5^\circ$, $a_{io}/(K_i/2) = 0.01$ and $a_{qo}/(K_i/2) = 0.006$. These are the RMS values taken from a custom–matched I/Q demodulator[6] over an operating instantaneous bandwidth of 100 MHz. The RMS values are small and are obtained after a mean value has been removed from each of the mismatch components. Different combinations of the four mismatch components are used to illustrate four specific cases; namely (i) amplitude and phase imbalance only, (ii) DC offsets only, (iii) amplitude imbalance and DC offset only and (iv) all four mismatches are present. The RMS and peak–to–peak normalized

instantaneous frequency deviations as a function of imbalances and DC offsets versus normalized signal frequency are plotted in Figs. 11 (a) and (b) respectively. For a given set of mismatches, the instantaneous frequency deviation for a continuous–time processor increases directly proportional to the baseband frequency as given by Eq.(18). However, as can be seen from Figs. 11 (a) and (b), the instantaneous frequency deviation for a discrete–time processor is not monotonically increasing with frequency. Depending on the relative values of the imbalances and DC offsets, the instantaneous frequency deviation may peak before the signal frequency reaches the sampling frequency. In the case where there are small amplitude and phase imbalances only, the period of the phase error is essentially half of that of the input phase cycle. As a result, when the baseband frequency is half that of the sampling frequency, the phase error is approximately the same at every sample point. Therefore the resultant instantaneous frequency deviation as given by Eq.(62) will be zero and thus the approximation used in deriving the instantaneous frequency actually reduces the effect due to the mismatches. For other combinations of imbalances and DC offsets, the net effect due to aliasing and approximation is more complex and their values as a function of frequency are shown by the other curves in the Figures.

To facilitate the comparison between the continuous–time processor and a discrete–time processor, Eq.(62) is multiplied by f_s/f to yield

$$\Delta f(t_n)/f = f_s/f \left[[a(t_n) - a_o(t_n)] - [a(t_{n-1}) - a_o(t_{n-1})] \right] /(2\pi) \tag{63}$$

where the total instantaneous frequency deviation has been normalized by the input baseband carrier frequency (f). With this normalized expression, it can be compared directly with the normalized instantaneous frequency deviation $[\partial a(t)/\partial a_o(t)]$ for a continuous–time processor. The normalized RMS instantaneous frequency deviation for the same sets of imbalances and DC offsets are plotted in Fig. 12. The normalized RMS instantaneous frequency deviations at $f/f_s = 0$ are identical to those from a continuous–time processor. The normalized instantaneous frequency deviation decreases with input frequency as shown, while for a continuous–time processor it is independent of input signal frequency. As a result, the normalized instantaneous frequency deviation for a discrete–time processor is always less than that of a continuous–time processor and this error is also decreasing with input frequency.

8.0 REDUCTION OF SYSTEMATIC ERRORS BY LOW–PASS FILTERING

The effects of imbalances and DC offsets on the envelope, phase and instantaneous frequency have been addressed. For a number of specific cases where two out of four possible mismatch components are present, a full characterization has also been given. In the general case, when all the mismatch components are present, the analysis can be more complicated. However, there are some general conclusions which can be made on the distortions introduced by the mismatches on input CW signals. For both the envelope in terms of peak–to–peak–ripple/mean and the normalized instantaneous frequency deviation, the mean is always zero over an input phase range of 2π radians. On the other hand, the mean for the phase error is not zero.

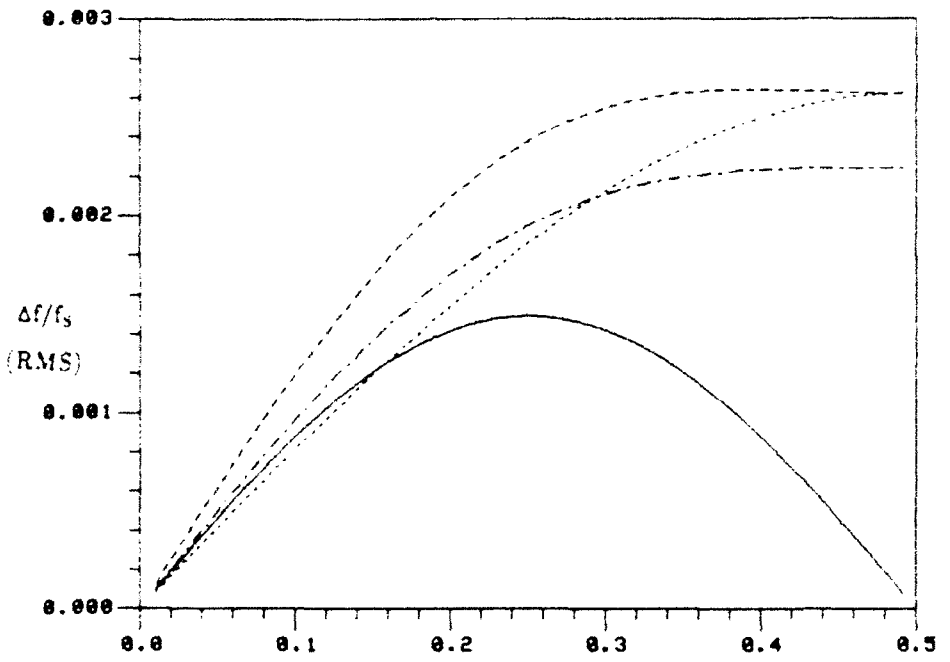

(a) RMS

——— $R = 1.01, \Delta\phi = 0.5^\circ, \; a_{io}/[a(t)K_i/2] = 0, \quad a_{qo}/[a(t)K_i/2] = 0$

····· $R = 1, \quad \Delta\phi = 0^\circ, \quad a_{io}/[a(t)K_i/2] = 0.01, \; a_{qo}/[a(t)K_i/2] = 0.006$

—·—·— $R = 1.01, \Delta\phi = 0^\circ, \quad a_{io}/[a(t)K_i/2] = 0.01, \; a_{qo}/[a(t)K_i/2] = 0$

– – – – $R = 1.01, \Delta\phi = 0.5^\circ, \; a_{io}/[a(t)K_i/2] = 0.01, \; a_{qo}/[a(t)K_i/2] = 0.006$

Figure 11 Normalized Instantaneous Frequency Deviation Versus Normalized Frequency

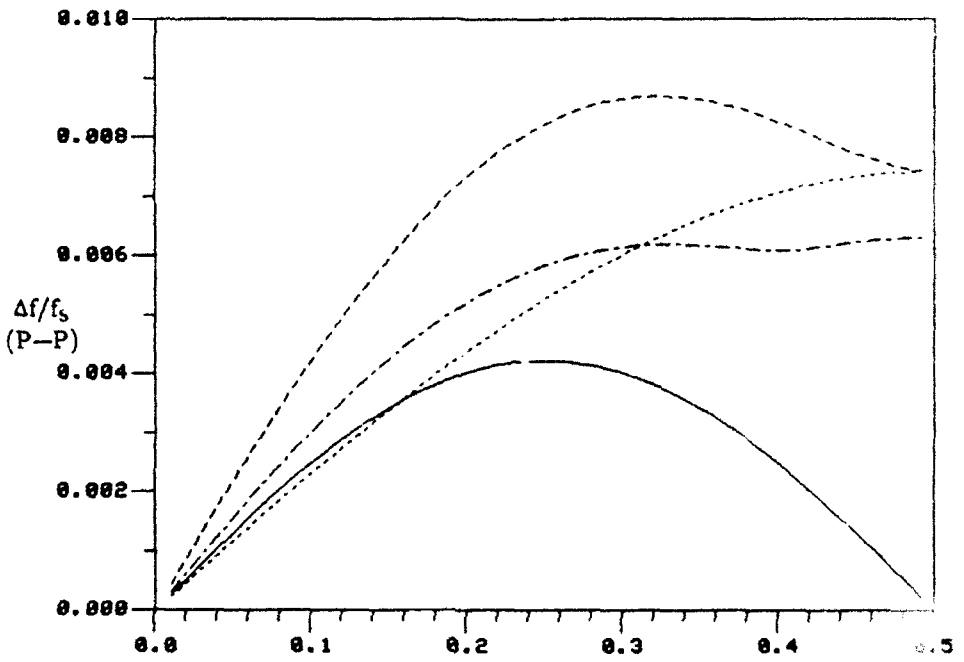

(b) Peak–to–peak

——— R = 1.01, $\Delta\phi = 0.5^\circ$, $a_{io}/[a(t)K_i/2] = 0$, $a_{qo}/[a(t)K_i/2] = 0$

····· R = 1, $\Delta\phi = 0^\circ$, $a_{io}/[a(t)K_i/2] = 0.01$, $a_{qo}/[a(t)K_i/2] = 0.006$

—·—·— R = 1.01, $\Delta\phi = 0^\circ$, $a_{io}/[a(t)K_i/2] = 0.01$, $a_{qo}/[a(t)K_i/2] = 0$

– – – – R = 1.01, $\Delta\phi = 0.5^\circ$, $a_{io}/[a(t)K_i/2] = 0.01$, $a_{qo}/[a(t)K_i/2] = 0.006$

Figure 11 Normalized Instantaneous Frequency Deviation Versus Normalized Frequency

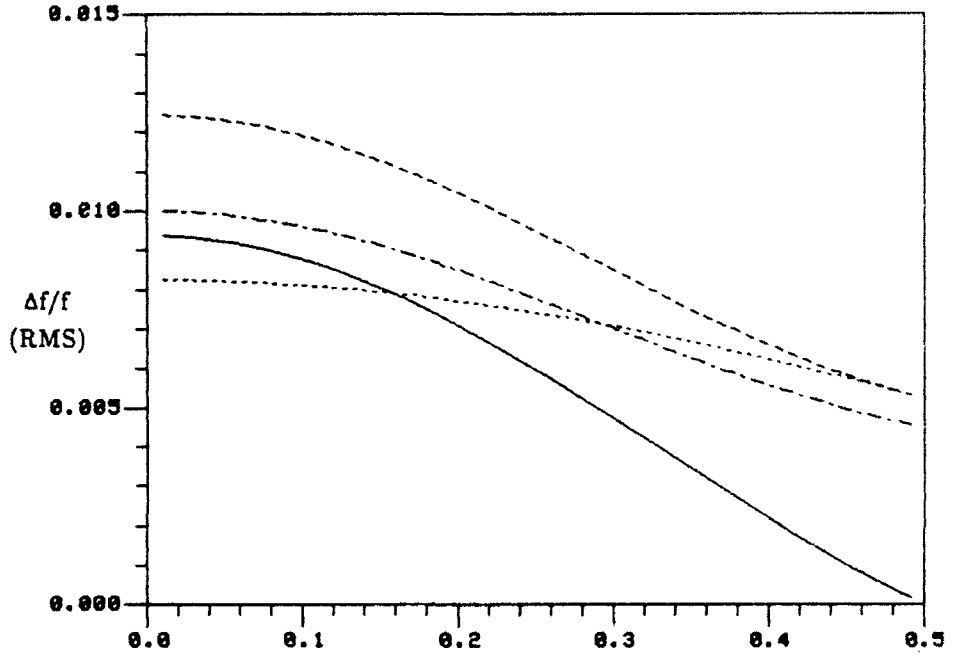

——— $R = 1.01, \Delta\phi = 0.5^{\circ}, \; a_{io}/[a(t)K_i/2] = 0, \quad a_{qo}/[a(t)K_i/2] = 0$

····· $R = 1, \quad \Delta\phi = 0^{\circ}, \quad a_{io}/[a(t)K_i/2] = 0.01, \; a_{qo}/[a(t)K_i/2] = 0.006$

—·—·— $R = 1.01, \Delta\phi = 0^{\circ}, \quad a_{io}/[a(t)K_i/2] = 0.01, \; a_{qo}/[a(t)K_i/2] = 0$

– – – – $R = 1.01, \Delta\phi = 0.5^{\circ}, \; a_{io}/[a(t)K_i/2] = 0.01, \; a_{qo}/[a(t)K_i/2] = 0.006$

Figure 12 Normalized Instantaneous Frequency Deviation Versus Normalized Frequency

For an input signal of constant amplitude, the distortions on the envelope produce a DC (bias) component which is only a function of the DC offsets and amplitude imbalance. In addition, a combination of sinusoidal components can also occur with periods equal to one and one half of the input phase cycle The bias due to DC offsets can also reduce the dynamic range of the demodulator. On the phase error, there are also a bias and AC components with periods equal to one and one half of the input phase cycle. There are also AC components with periods equal to one and one half of the input phase on the instantaneous frequency deviation, however there is no bias. As the magnitudes of the imbalances and DC offsets increase, the AC components for both the phase error and instantaneous frequency deviation will depart further from a sinusoidal waveform.

Two examples are used to show the frequency spectral distribution of the distortion as a function of imbalances and DC offsets. A CW baseband signal at a normalized frequency (f/f_s) of 0.05 and with a power of 0 dBm in a 50–Ohm system is used. The distortions on both the envelope and instantaneous frequency due to the imbalances and DC offsets are then calculated. 1000 sample points taken on the distortions are used for the discrete Fourier transform. The frequency of the CW signal is chosen so that minimal aliasing and leakage can occur. The normalized one–sided spectral distributions on both the envelope and instantaneous frequency are plotted in Figs. 13 and 14. The spectral distribution on the envelope is normalized by the power of the undistorted envelope and is then expressed in dB. The instantaneous frequency deviation is normalized by the Nyquist sampling rate and the ratio is also expressed in dB [$10 \cdot LOG_{10}(\Delta f/f_s)$]. The spectral distributions plotted in Fig.13 are obtained by using typical mismatch values from a custom–matched I/Q demodulator[6] while in Fig. 14, the mismatches are increased by a factor of ten. As expected, there are only three spectral components on the envelope distortions due to the mismatches; namely the DC component and the fundamental and second harmonics of the baseband frequency. For the normalized instantaneous frequency deviation, there is no DC component. For small imbalances and DC offsets, only the fundamental and second harmonic frequency components are present. For larger mismatches, other higher harmonics also occur.

As can be seen from Fig. 13, the distortions on the envelope are very small and are quite acceptable for EW applications. From Fig. 11, the instantaneous frequency error is quite small when the input baseband frequency is low. However, as the signal frequency is increased, the instantaneous frequency deviation also gets larger. This relatively large instantaneous frequency error may not be acceptable and some improvement may be needed.

As discussed earlier, for EW applications the video or modulating bandwidths of both the envelope and instantaneous frequency are usually small in comparison to the instantaneous frequency bandwidth of the I/Q demodulator. In addition, as shown in Fig. 13, the distortions are usually made up of frequency components which are harmonics of the baseband signal frequency. As a result, when a signal is down–converted to a high baseband frequency low–pass filtering can be effectively applied to reduce the high frequency components of the distortions. Another advantage of reducing the video bandwidth by low–pass filtering is a reduction in the effective noise bandwidth[14] which will result in an improvement on the output signal–to–noise ratio. In other words, the effective noise bandwidth of an I/Q demodulator is a function of both its instantaneous bandwidth and its video bandwidth.

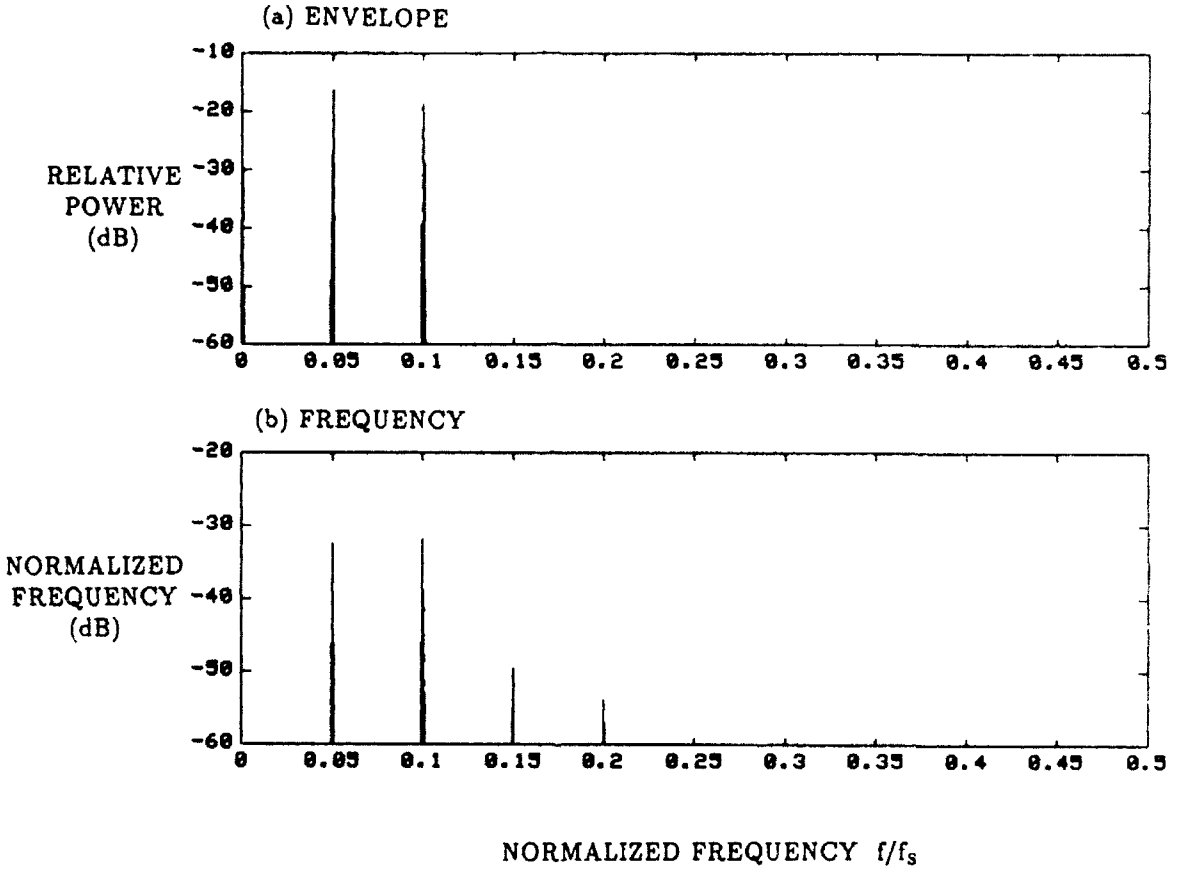

Figure 13 Frequency Spectral Distribution of Envelope Distortion and Instantaneous Frequency Deviation ($R = 1.01$, $\Delta\phi = 0.5^{\circ}$, $a_{io}/[a(t)K_i/2] = 0.01$ and $a_{qo}/[a(t)K_i/2] = 0.006$)

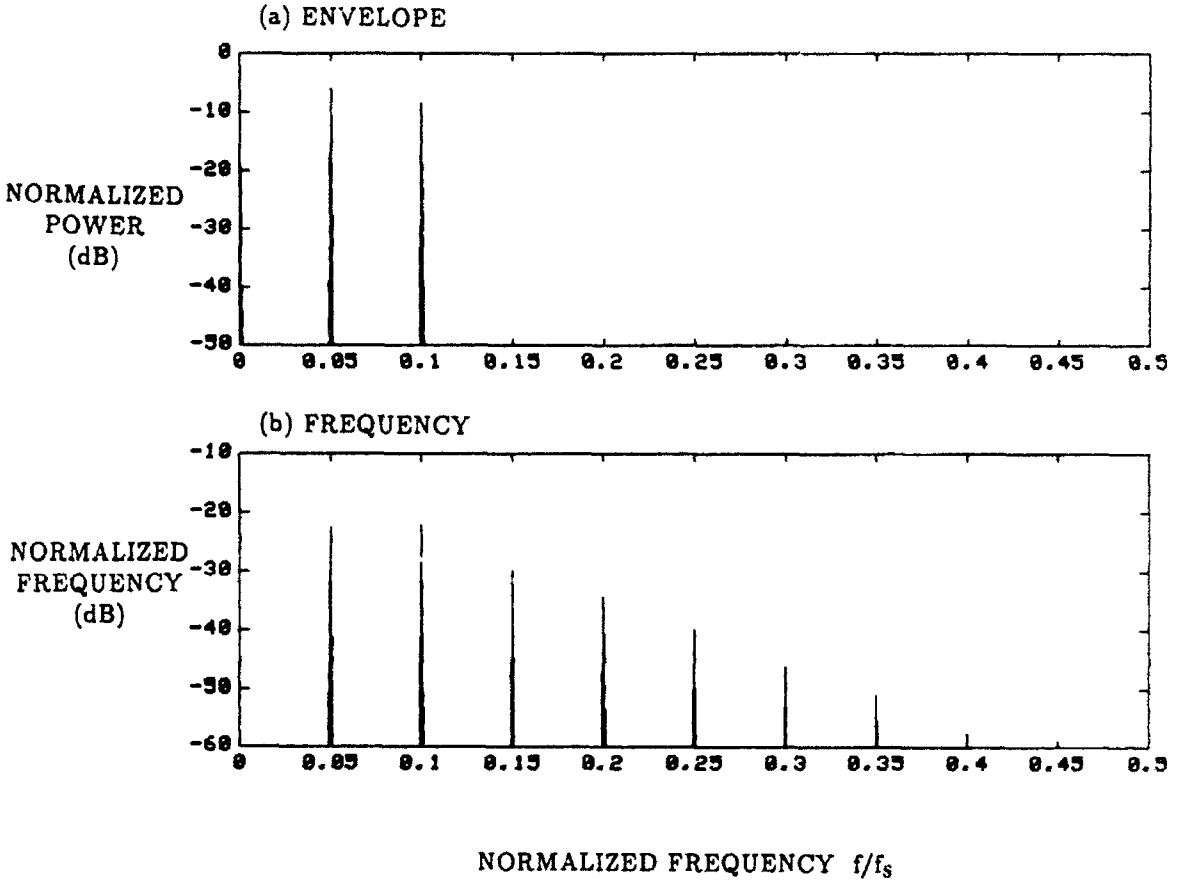

Figure 14 Frequency Spectral Distribution of Envelope Distortion and Instantaneous Frequency Deviation (R = 1.10, $\Delta\phi = 5^{\circ}$, $a_{io}/[a(t)K_i/2] = 0.1$ and $a_{qo}/[a(t)K_i/2] = 0.06$)

Simple low–pass filtering can be carried out in the time domain by using a moving average. It is carried out by adding N contiguous samples and an average is taken on the accumulated sum. The same operation is repeated on the next N samples. The transfer function is given by[9]

$$H(f)/N = \sin(N\pi fT_s)/\ [N \sin(\pi fT_s)]\ \exp\ [\ -j(N-1)\pi fT_s\ ] \qquad (64)$$

The absolute value of the transfer function is plotted in Fig.15(a) for various values of N. As can be seen from the plot, the operation of moving average on the sampled, processed data has the same effect as low–pass filtering in the frequency domain. In addition, the moving average is easy to implement digitally and is of linear phase response which does not introduce distortions such as ringing and overshoot as for some other types of filters [15]. As given in Fig. 15(a), the sidelobe levels are determined by Eq.(64) as a function of N. For large N, the first peak sidelobe level is 13.46 dB down and the peak sidelobe level decreases directly proportional to 1/f. If it is desirable to have lower sidelobe levels, a multi–layer moving average can be performed. Fig.15 (b) shows the resultant effect when two layers are used. In this case the data is filtered by a moving average of N = 3 and followed by N = 4. Moreover, if more stringent requirement is needed, FIR filters with generalized linear phase can easily be designed [9]. The tradeoff is the increased complexity in hardware implementation.

Two examples are given to illustrate the effectiveness of low–pass filtering. A linear FM signal centered at a baseband frequency of 25 MHz ($f/f_s = 0.25$) with a total frequency excursion of 5 MHz is used. The pulse width is 1 μs with rise and fall time constants of 0.02 μs. The power of the envelope and instantaneous offset (from the LO frequency) frequency of the signal are plotted in Fig. 16. At the very beginning and end of the pulse, there is an abrupt change in the phase of the signal which shows up as a spike in the instantaneous frequency. As the instantaneous frequency inside the pulse varies, the frequency of the ripples will also vary as shown. In the first half of the pulse, the frequency components of the ripples which mainly composed of the first and second harmonics of the baseband frequency are less than half the Nyquist sampling frequency. In the second half of the pulse, the frequency of the second harmonic exceeds the Nyquist sampling frequency and as a result, aliasing will occur. Fig. 17 shows the result after two layers of moving average are applied. Since the modulating bandwidth of the linear FM signal is much less than its baseband carrier frequency, low–pass filtering can be effectively used to attenuate the ripples with minimal effect on the demodulated envelope and instantaneous frequency. It is noted that both the leading and trailing edges of the pulse are slightly rounded due to low–pass filtering. In a practical system, adaptive low–pass filtering with different degrees of smoothing can be applied to different parts of the pulse to minimize this type of distortion. In this case, if it is desirable to retain the high frequency components of the demodulated information at both the leading and trailing edges, then no low–pass filtering should be applied near either the leading or trailing edge.

9.0 SUMMARY AND CONCLUSIONS

The effects of imbalances and DC offsets in an I/Q demodulator for the demodulation of radar signals have been analyzed in this report. Three normalized parameters, namely the peak–to–peak–ripple to mean, phase error and normalized instantaneous frequency deviation have been used to characterize the systematic errors on

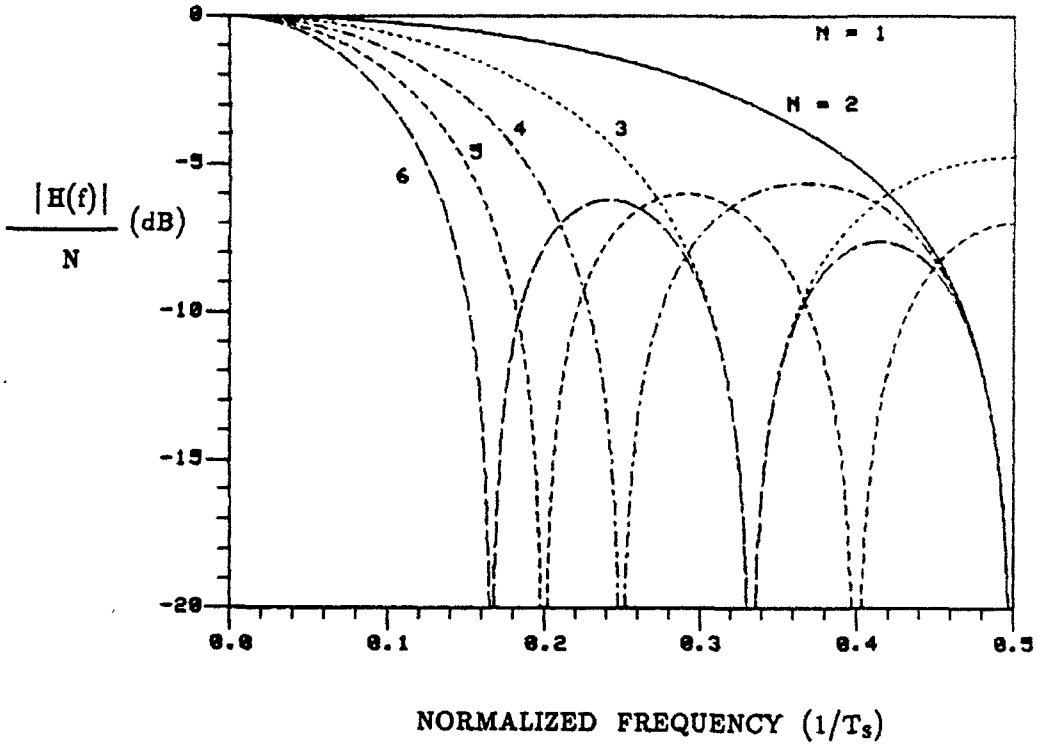

(a) Single Layer

Figure 15 Transfer Function of Moving Average

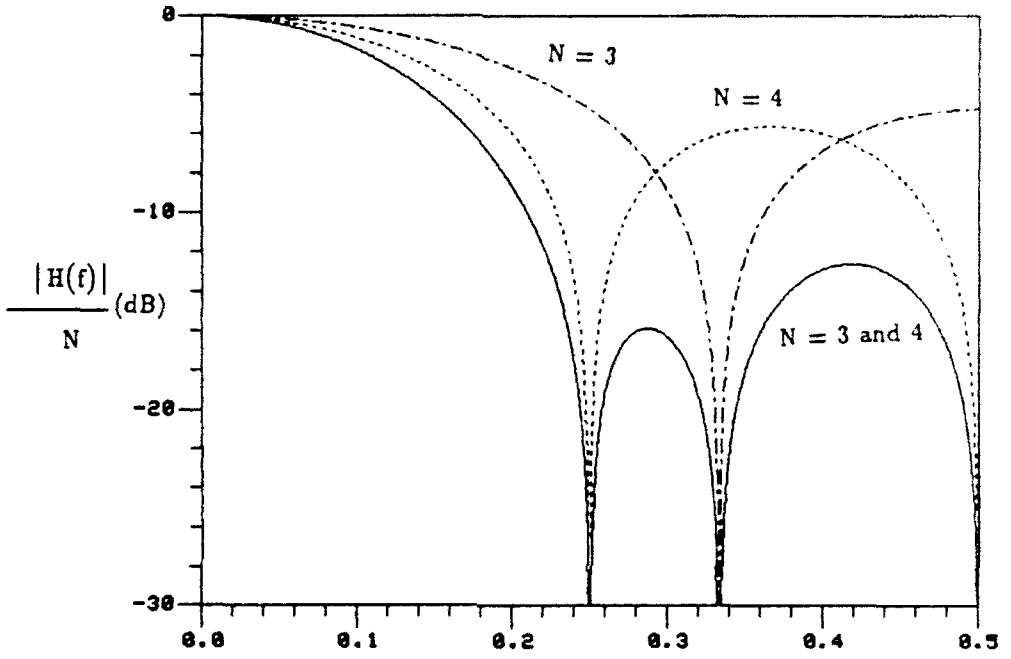

(b) Two Layers

Figure 15 Transfer Function of Moving Average

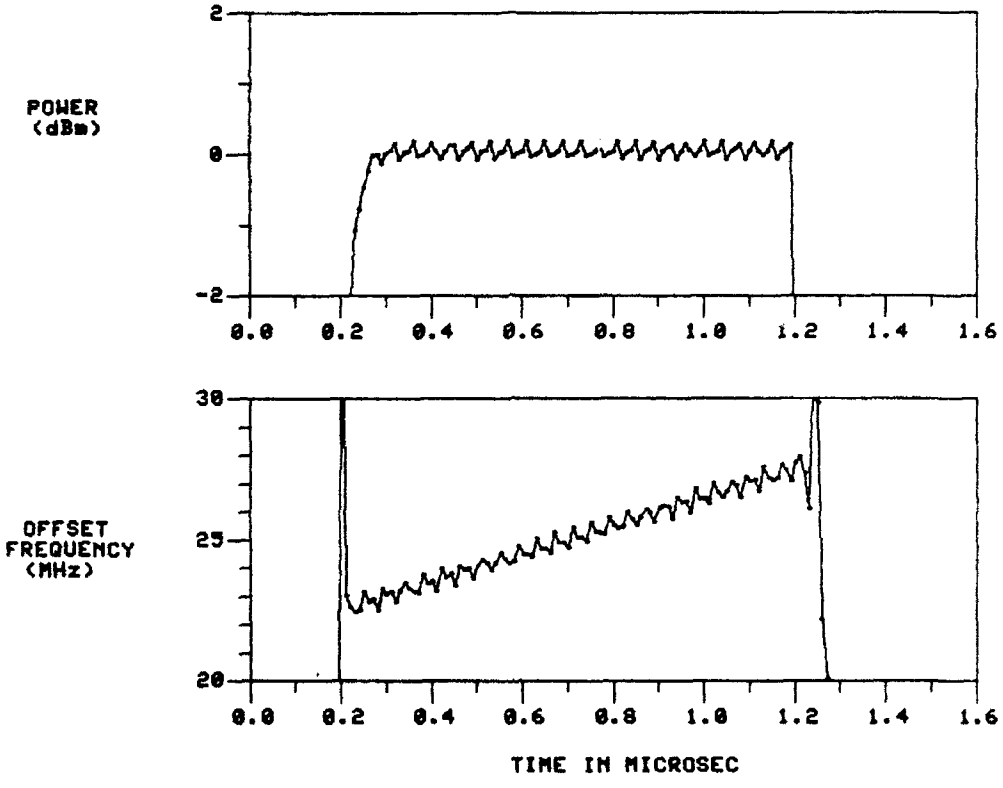

Figure 16 Raw Data of Envelope and Instantaneous Offset Frequency of a Linear FM Signal (Pulse Width = 1 μs, Baseband Frequency= 25 MHz, Δf = 5 MHz and T_s = 10 ns)

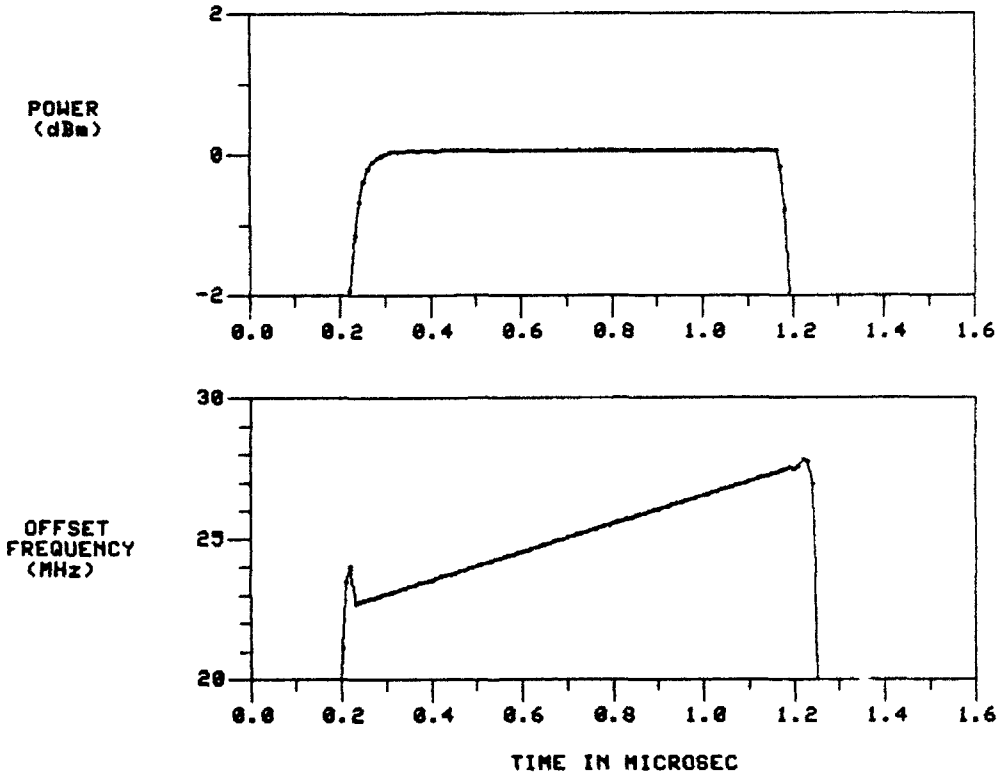

Figure 17 Envelope and Instantaneous Offset Frequency of a Linear FM Signal with Low–pass Filtering (3 and 4–point Moving Averages, Pulse Width = 1 μs, Baseband Frequency = 25 MHz, Δf = 5 MHz and T_s = 10 ns,)

the demodulated envelope, phase and instantaneous frequency respectively. These parameters are evaluated as a function of imbalances and DC offsets over an input phase range of 2π radians.

When there are imbalances and DC offsets in the I/Q demodulator, the power of the envelope is found to be a product of the undistorted envelope term and other terms which are generated by the imbalances and DC offsets. When the amplitude of the input signal is constant, distortions in the form of a DC (bias) component is produced on the envelope and this bias is only a function of DC offsets and amplitude imbalance. In addition, a combination of sinusoidal components with frequencies equal to the fundamental and second harmonics of the baseband signal frequency can also occur. The bias due to DC offsets can also reduce the dynamic range of the demodulator. On the phase error, there are also a bias and AC components with periods equal to one and one half of the input signal phase. Similarly, there are also AC components on the instantaneous frequency deviation, however, there is no bias. As the magnitudes of the mismatches increase, the AC components for both the phase error and instantaneous frequency deviation will depart further from a purely sinusoidal waveform.

In a discrete–time processor, the input signals are sampled, quantized and processed with a finite bandwidth which is limited by the Nyquist sampling rate. In a non–ideal I/Q demodulator where there are imbalances and DC offsets, frequency components higher than the Nyquist sampling rate can be generated by the non–linear operations of computing the power of the envelope and its phase. As a result, aliasing can occur and large errors can also result in the determination of the phase. Another factor which can affect the instantaneous frequency measurement is the approximation used by taking the difference between two contiguous phase samples and then dividing the difference by the sampling interval. The effect due to aliasing and approximation is a function of input signal frequency, imbalances and DC offsets. For a given set of imbalances and DC offsets, the instantaneous frequency deviation for a continuous–time processor increases directly proportional to the baseband frequency. However, the instantaneous frequency deviation for a discrete–time processor is not monotonically increasing with frequency. Depending on the relative values of the imbalances and DC offsets, the instantaneous frequency deviation may peak before the frequency reaches the sampling frequency. As a result, the instantaneous frequency deviation in a discrete–time processor is always less than that of a continuous–time processor.

In EW applications, the video or modulation bandwidth of the signal is usually small in comparison to the instantaneous frequency bandwidth of the I/Q demodulator. As a result, when the signal is down–converted to a baseband frequency which is larger than the modulation bandwidth, the frequency components of the distortions can be reduced by low–pass filtering. The technique of using a moving average has been shown to be effective to attenuate the ripples caused by the mismatches and with minimal effect on both the demodulated envelope and instantaneous frequency.

10.0 REFERENCES

[1] Tsui, J.B.Y. *Digital Microwave Receivers*. Norwood, MA: Artech House, 1989.

[2] Wiley, R.G. *Electronic Intelligence: The Interception of Radar Signals.* Norwood, MA: Artech House, 1985.

[3] Sharpin, D.L., Tsui, J.B.Y., and Hedge, J. The Effects of Quadrature Sampling Imbalances on a Phase Difference Analysis Technique. Proceedings of the IEEE, National Aerospace and Electronics Conference, NAECON 1990, Vols. 1–3; 962–968, New York.

[4] Goldman, S.J. Understanding the limits of quadrature detection. Microwave & RF, 67–70, Dec, 1986.

[5] Roome, S.J. Analysis of quadrature detectors using complex envelope notation. In IEE proceedings, Vol. 136, Pt. F, No.2, April 1989.

[6] Lee, J.P.Y. I/Q demodulation of radar signals with calibration and filtering DREO report 1119, Defence Research Establishment Ottawa, Department of National Defence, Canada.

[7] Anaren Microwave Inc. Catalog No. 17A

[8] Churchill, F.E., Ogar, G.W. and Thompson, B.J. The correction of I and Q errors in a coherent processor. IEEE Trans. Aerospace and electronic systems. Vol. AES–17, No.1, Jan, 1981.

[9] Oppenheim, A.V. and Schafer, R.W. *Discrete-time Signal Processing.*

[10] Rice, D.W. and Wu, K.H. Quadrature Sampling with High Dynamic Range. IEEE Trans. AES, Vol. 18, No.4, 736–739, Nov,1982

[11] Radar, C.R. A Simple Method for Sampling In–phase and Quadrature Components. IEEE Trans. AES, Vol. 20, No.6, 821–824, Nov, 1984.

[12] Bortot, P. Complex Demodulation Using a Digital Technique. Technical Report, Interactive Circuits and Systems Ltd Ottawa, Canada, Dec, 1986

[13] Brigham, E. Oran. *The Fast Fourier Transform.* Englewood Cliffs, New Jersey: Prentice–Hall, 1974.

[14] Lucas, W.J. Tangential sensitivity of a detector video system with R.F. pre–amplification. In Proc. IEE, Vol. 113, No.8, 1321–1330, August 1966.

[15] Johnson, D. E. *Introduction to Filter Theory.* Englewood Cliffs, New Jersey: Prentice–Hall, 1976.

DOCUMENT CONTROL DATA

(Security classification of title, body of abstract and indexing annotation must be entered when the overall document is classified)

1. ORIGINATOR (the name and address of the organization preparing the document. Organizations for whom the document was prepared, e.g. Establishment sponsoring a contractor's report, or tasking agency, are entered in section 8.)

DEFENCE RESEARCH ESTABLISHMENT OTTAWA
NATIONAL DEFENCE
SHIRLEY BAY, OTTAWA, ONTARIO K1A 0K2 CANADA

2. SECURITY CLASSIFICATION (overall security classification of the document, including special warning terms if applicable)

UNCLASSIFIED

3. TITLE (the complete document title as indicated on the title page. Its classification should be indicated by the appropriate abbreviation (S,C or U) in parentheses after the title.)

EFFECTS OF IMBALANCES AND DC OFFSETS ON I/Q DEMODULATION (U)

4. AUTHORS (Last name, first name, middle initial)

LEE, JIM P.

5. DATE OF PUBLICATION (month and year of publication of document)	6a. NO. OF PAGES (total containing information. Include Annexes, Appendices, etc.)	6b. NO. OF REFS (total cited in document)
DECEMBER 1992	47	15

7. DESCRIPTIVE NOTES (the category of the document, e.g. technical report, technical note or memorandum. If appropriate, enter the type of report, e.g. interim, progress, summary, annual or final. Give the inclusive dates when a specific reporting period is covered.)

DREO REPORT

8. SPONSORING ACTIVITY (the name of the department project office or laboratory sponsoring the research and development. Include the address.)

DEFENCE RESEARCH ESTABLISHMENT OTTAWA
NATIONAL DEFENCE
SHIRLEY BAY, OTTAWA, ONTARIO K1A 0K2 CANADA

9a. PROJECT OR GRANT NO. (if appropriate, the applicable research and development project or grant number under which the document was written. Please specify whether project or grant)	9b. CONTRACT NO. (if appropriate, the applicable number under which the document was written)
011LB11	

10a. ORIGINATOR'S DOCUMENT NUMBER (the official document number by which the document is identified by the originating activity. This number must be unique to this document.)	10b. OTHER DOCUMENT NOS. (Any other numbers which may be assigned this document either by the originator or by the sponsor)
DREO REPORT 1148	

11. DOCUMENT AVAILABILITY (any limitations on further dissemination of the document, other than those imposed by security classification)

(X) Unlimited distribution
( ) Distribution limited to defence departments and defence contractors; further distribution only as approved
( ) Distribution limited to defence departments and Canadian defence contractors; further distribution only as approved
( ) Distribution limited to government departments and agencies; further distribution only as approved
( ) Distribution limited to defence departments; further distribution only as approved
( ) Other (please specify):

12. DOCUMENT ANNOUNCEMENT (any limitation to the bibliographic announcement of this document. This will normally correspond to the Document Availability (11). However, where further distribution (beyond the audience specified in 11) is possible, a wider announcement audience may be selected.)

UNLIMITED

UNCLASSIFIED

SECURITY CLASSIFICATION OF FORM

13. ABSTRACT (a brief and factual summary of the document. It may also appear elsewhere in the body of the document itself. It is highly desirable that the abstract of classified documents be unclassified. Each paragraph of the abstract shall begin with an indication of the security classification of the information in the paragraph (unless the document itself is unclassified) represented as (S), (C), or (U). It is not necessary to include here abstracts in both offical languages unless the text is bilingual).

(U) The effects of imbalances and DC offsets, in an I/Q demodulator, on the demodulation of radar signals are addressed in this report. Three normalized parameters, namely the peak-to-peak-ripple to mean, phase error and normalized instantaneous frequency deviation are used to characterize distortions introduced on the envelope, phase and instantaneous frequency respectively. The effect on the distortions, due to aliasing and approximation use in deriving the instantaneous frequency in a discrete-time processor, is also analyzed.

(U) When there are imbalances and DC offsets, a bias is produced on both the demodulated envelope and phase. AC ripples with frequency components which are multiples of the baseband frequency are also generated on all of the three demodulated signal waveforms. In EW applications, the instantaneous bandwidth of the I/Q demodulator is usually much wider than the demodulated signal bandwidth. As a result, when the baseband frequency of the signal is high and comparable to its modulation bandwidth, the higher frequency components of the distortion can be effectively reduced by low-pass filtering.

14. KEYWORDS. DESCRIPTORS or IDENTIFIERS (technically meaningful terms or short phrases that characterize a document and could be helpful in cataloguing the document. They should be selected so that no security classification is required. Identifiers, such as equipment model designation, trade name, military project code name, geographic location may also be included. If possible keywords should be selected from a published thesaurus, e.g. Thesaurus of Engineering and Scientific Terms (TEST) and that thesaurus-identified. If it is not possible to select indexing terms which are Unclassified, the classification of each should be indicated as with the title.)

I/Q DEMODULATION
RADAR ESM
DIGITAL RECEIVER
RADAR SIGNAL PARAMETER MEASUREMENT

UNCLASSIFIED

SECURITY CLASSIFICATION OF FORM